Transfer at *C. elegans* synapses

Thesis by

Anusha Narayan

In Partial Fulfillment of the Requirements

for the Degree of

Doctor of Philosophy

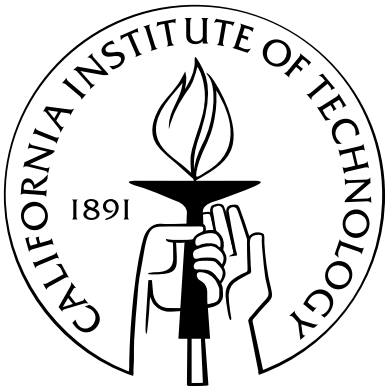

California Institute of Technology

Pasadena, California

2010

(Submitted 17 March 2010)

for my parents

Acknowledgements

I'd like to begin by thanking my two advisors. I hope I can absorb a fraction of Paul Sternberg's unique blend of energetic enthusiasm and level-headed pragmatism, and I very much appreciate his way of making sure I always had the support and resources I needed. Earning my experimental spurs in the laboratory of Gilles Laurent was a formative experience, and I learned much from his approach to science and his knowledge of physiology. Together, they made sure I always had a safety net even as I was out on a limb, sawing madly; when the going was rough their support and concern was extraordinary.

Thanks are also due to my committee: Shuki Bruck, who was supportive and encouraging from my earliest days at Caltech; Erin Schuman who was always interested, and never short of ideas and suggestions; and Thanos Siapas, who was always available, concerned and supportive.

Having two advisors meant that I was lucky enough to work with two great groups of people: the Sternberg and Laurent labs, who blended to a nicety inspiring science and goofy fun. In particular, I would like to thank Vivek Jayaraman and Glenn Turner for their friendship, for being always generous with their time and counsel, and for being such shining exemplars of Reasonable Assumptions and Gomey-Bubbles respec-

tively. Maria ('ain't no mountain high enough') Papadopoulou and Stijn Cassenaer are surrogate family; they are textbook examples of grace under pressure; and the opportunity to see them at work, blending insight with a virtuoso command of technique, was one of the scientific highlights of my time in grad school. Watching Cindy Chiu take on and conquer tasks of incredible complexity was always inspirational, as was Eric Mosser's ability to maintain an even keel: I would like to thank them both for their support and friendship. I tremendously enjoyed cahooting with Melanie Pribisko Yen and the Eating Club, combining our collective passion for talking and eating. I would like to thank Ofer Mazor and Benjamin Rubin for innumerable highly enjoyable conversations running the gamut from slow microprocessors to water-buffaloes bellowing across a swamp. I would also like to thank the many good friends from the early weeks of international student orientation who have enriched my life at Caltech. In particular, I would like to thank Rogier Braakman, for his support, his calm good sense, his cheerful patience, and a number of other things. And finally, I would like to thank my parents. I would not be at Caltech without them, and I will always be grateful for all they have done for me.

Abstract

The nematode *C.elegans*, with its 302 neurons and abundance of genetic, laser ablation, electrophysiological and imaging tools, is a compact and attractive system for neural circuit analysis. An understanding of the functional dynamics of neural computation requires physiological analyses. We undertook the first characterization of transfer at central synapses in *C.elegans*. To achieve this we employed optical stimulation techniques using channelrhodopsin-2, and combined this with whole-cell patch clamp electrophysiological recording techniques. We show that the synapse between AFD and AIY, the first stage in the thermotactic circuit, exhibits excitatory, tonic and graded release. The gain at the synapse was low (<0.1), and release was frequency independent, showing no signs of facilitation or depression. The AFD-AIY synapse thus seems designed for robust and reliable transmission of a scaled-down temperature signal from AFD to AIY, enabling AIY to continuously monitor temperature information and integrate it with other incoming sensory information. We also investigated the synapse between ASER, a chemosensory neuron, and AIY, and found that the synaptic response was small and inconsistent. The combination of optical stimulation tools with neural recording techniques is a powerful way to analyze neural circuitry, and will be a significant aid in achieving the goal of understanding how

information is processed in the compact yet densely interconnected nervous system of the worm.

Contents

List of Figures

Chapter 1

Introduction

From the perspective of systems neuroscience, a small nervous system with access to a multiplicity of tools to selectively perturb and analyze the activity of ensembles of neurons has tremendous appeal. *C. elegans*, with its three-hundred odd neurons, is one such system.

1.1 The anatomy and nervous system of the nematode *C. elegans*

C. elegans is a roundworm, one of around 30,000 species belonging to the Phylum *nematoda*. It is a free-living soil nematode feeding on bacteria, about 2-3 mm in length when full grown, and has fewer than a thousand cells in total. Of these, 302 are neurons in the hermaphrodite (there are both males and hermaphrodites in *C. elegans*). The male has 79 additional neurons, nearly all of which are involved in control of mating. It takes around three days for a worm to grow from egg to adult, and the average lifespan of a worm is around two weeks.

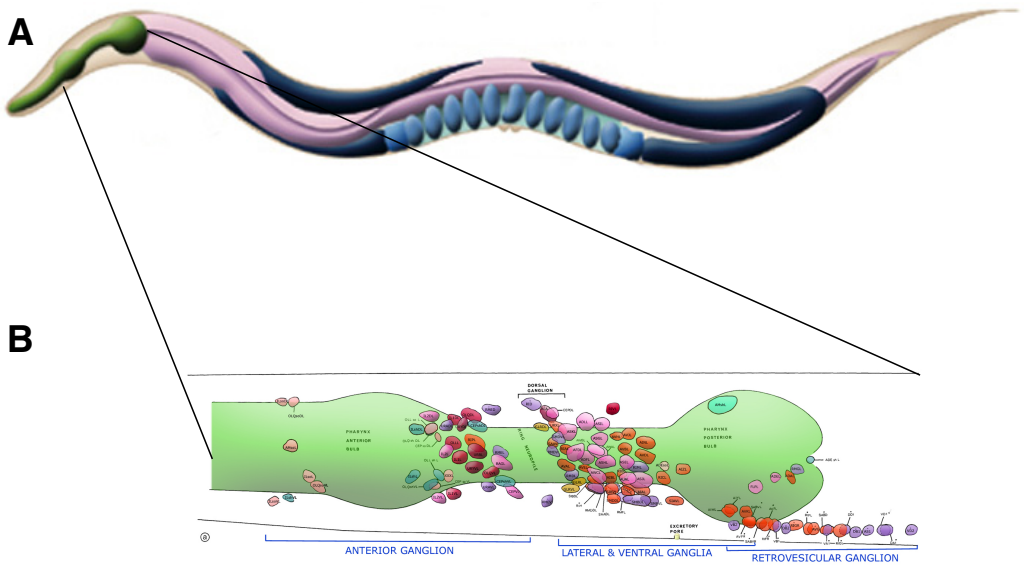

Figure 1.1: The worm nervous system. A. Schematic representation of a gravid adult hermaphrodite worm. Eggs are labelled in blue and the pharynx in green. B. Schematic representation of neuronal cell bodies clustered in ganglia around the pharynx. The blank space between the anterial and the lateral/ventral ganglia is taken up by the neuropil in the nerve ring. Figure adapted with permission from WormAtlas (Altun & Hall, 2008).

The body of a worm is an unsegmented cylindrical tapered tube with a tough cuticle covering the hypodermis (see Figure 1.1A). Body shape is maintained by high internal pressure - the worm will explode open when cut. *C. elegans* is a filter feeder, taking in a mixture of bacteria and water through its mouth, passing it through the pharynx which grinds and filters out the food into the intestine. A worm will typically crawl through its environment with a characteristic sinusoidal locomotory pattern, and slow down on a lawn of food or in the presence of potential mates.

The three hundred-odd neurons of the worm are partitioned into two systems. The pharyngeal nervous system comprises about 20 neurons and autonomously controls the alimentary system. The remaining neurons comprise the somatic nervous system, and their cell bodies are organized into ganglia in the head and tail. Figure 1.1B shows the primary ganglia in the head of the worm. The nerve ring, the primary

neuropil of the worm, is a synapse-rich band of processes that wraps around the pharynx of the worm. A subset of neurons, primarily motor neurons controlling the contraction and expansion of the body wall muscles involved in the characteristic sinusoidal movement of the worm, are studded along the ventral midline. There are two nerve cords - dorsal and ventral, that carry the processes of most neurons from the posterior part of the worm as they project to the nerve ring. There are approximately 6400 chemical synapses, 900 gap junctions and 1500 neuromuscular junctions (Altun et al., 2002-2009).

1.2 Worm behavior

For its small size and compact nervous system, the worm exhibits a range of behaviors (de Bono & Maricq, 2005). In addition to executing functions such as locomotion, mating and egg-laying, a worm will exhibit preferences in temperature, the valence and concentration of chemicals, and mechanosensory environment. When placed in a shallow thermal, chemical, or electrical gradient, worms will migrate towards preferred zones consistently and reproducibly, based on initial conditions and past history (Hedgecock & Russell, 1975, Ward, 1973, Sukul & Croll, 1978). A worm will respond to negative stimuli such as a harsh mechanical touch, or aversive chemicals by backing away rapidly. Worms also display social feeding behavior (de Bono, 2003) as well as basic forms of learning such as habituation and paired conditioning (Giles et al., 2006). Food modulates many of these behaviors (Zhang et al., 2005).

1.3 The worm toolkit

There is a plethora of available tools that make *C. elegans* an attractive model system for neural circuit analysis. First of all, its small size and short generation time make it appealing as a laboratory animal. Additionally, it's transparent body allows live imaging of neuronal activity and tissue in intact animals. The full genome of *C. elegans* is available, giving us a remarkably high degree of genetic control over targeting and characterizing specific neurons. Perhaps most striking of all, it is the only animal for which we have detailed and complete reconstructions of the entire nervous systems using electron microscopy. Electrophysiological techniques have been developed to address questions of neural function with high temporal resolution. Calcium imaging studies are aided by the transparent body of the worm, and allow monitoring of neural activity remotely during awake behavior. In addition, the development of remote optical stimulation techniques add a powerful tool to the already impressive *C. elegans* collection.

1.4 Remote optical control of neural circuitry

Recent years have seen the development of techniques to control neurons remotely and optically. Nagel and colleagues first characterized the algae-derived cation channel channelrhodopsin. It is a microbial-type rhodopsin (a seven-transmembrane retinal protein that has no sequence homology to animal rhodopsins), derived from the green alga *Chalmydomonas reinhardtii*. Channelrhodopsin1 is a proton selective light

switched ion channel (Nagel et al., 2002); Channelrhodopsin2 (ChR2) is a leaky proton pump that can act as a mixed-cation light gated ion channel (Nagel et al., 2003, Feldbauer et al., 2009), and triggers larger currents. The cofactor all-*trans* retinal is required. The ChR2 conductance has an initial large transient value and decays to a lower stable steady state level with continued light illumination; the recovery of the peak current is faster at low extracellular pH or at more negative voltages. The estimated conductance of the channel is low, around 50 fS. The rise time of the ChR2 current is extremely fast: less than 200 μs; decay is on the order of milliseconds and is pH sensitive (Nagel et al., 2003). The peak of the ChR2 action spectrum is $\sim$460 nm.

Initial studies expressing ChR2 in cultured hippocampal neurons showed that this channel could be used to control neuronal spiking and synaptic transmission (Boyden et al., 2005). Since then, ChR2 has been used to control neural activity in a broad range of model systems, including worms, flies, fish, rodents and primates (Nagel et al., 2005, Schroll et al., 2006, Arenkiel et al., 2007, Huber et al., 2008, Douglass et al., 2008, Han et al., 2009).

The use of ChR2 can be extended to awake behaving conditions, and can drive behavior: in *C. elegans*, it was shown to be able to trigger behavioral responses (Nagel et al., 2005). Conveniently, worms can be fed the cofactor all-*trans* retinal. Worms expressing functional ChR2 in mechanosensory neurons responded to pulses of blue light with the rapid withdrawal/ acceleration responses typical of mechanical stimulation. In *Drosophila* larvae, light-induced activation of dopaminergic or

octopaminergic neuronal populations was found to substitute for reinforcing stimuli during olfactory learning (Schroll et al., 2006). ChR2-expressing neurons in mice could be stimulated and neuronal firing responses monitored using in vivo electrophysiological recording techniques (Arenkiel et al., 2007). Mice trained to associate water rewards with photostimulation of ChR2 expressing neurons (comprising $< 1\%$ of the cells in layer 2-3 of barrel cortex) were able to report photostimulation (Huber et al., 2008), and zebrafish with ChR2 in somatosensory neurons display escape behavior to blue light (Douglass et al., 2008). ChR2 has been used to induce long-term potentiation (LTP) in rat hippocampal slices (Zhang & Oertner, 2007).

Down the line, therapeutic and prosthetic applications may be possible: functional ChR2 has been expressed in the brain of the rhesus macaque, and used to mediate stimulation of cortical areas for months (Han et al., 2009), and ChR2 can be used to impart photosensitivity to inner retinal cells in mice with photoreceptor degeneration (Bi et al., 2006), restoring the ability of the retina to encode and transmit light signals to visual cortex.

Additionally, ChR2 has been used for anatomical tracing of projections and circuit mapping (Petreanu et al., 2007, Cruikshank et al., 2010), and in worms, it has been used to study release at the neuromuscular junction(Liewald et al., 2008, Liu et al., 2009).

The same logic of light-driven neuronal control can be extended to perform the complementary function: switching off neurons. Halorhodopsin is a yellow-light activated chloride pump derived from the archaebacterium *Natronomas pharaonis* that

can be used to silence cells with millisecond-timescale precision (Han & Boyden, 2007). Additionally, chimeric proteins of opsins with various receptors involved in intracellular signaling have been developed (Airan et al., 2009), further increasing the possible uses of remote control of cellular signaling.

The use of optical stimulation techniques has opened up many exciting possibilities for the control and selective manipulation of neural circuits, and in combination with electrophysiology can be used to address fundamental questions of neural coding.

1.5 Electrophysiology in the worm

The earliest electrophysiology from a nematode was an analysis of the locomotor circuit in the worm *Ascaris lumbricoidis* (Walrond et al., 1985, Walrond & Stretton, 1985a,b, Davis & Stretton, 1989a,b). Neurons in *Ascaris* are large - around 80-100 μm in diameter. Motor neurons in *Ascaris* were found to exhibit graded active and synaptic responses, and tonic synaptic release (Davis & Stretton, 1989a). Through simultaneous recordings of motor neurons and the muscles they innervate, the locomotor circuit was found to employ reciprocal inhibition to produce a sequence of alternating contractions of the worm body, enabling its characteristic sinusoidal movement pattern (Walrond & Stretton, 1985b). Given the striking anatomical similarities between the locomotory circuit in *Ascaris* and *C. elegans*, these studies were very informative in assessing the excitatory and inhibitory function of specific motor neurons in *C. elegans*.

Electrophysiology has historically been challenging in *C.elegans*, for several rea-

sons. The worm is a couple of millimeters in length, with very small neurons, averaging 2-3 μm in diameter. The body of the worm is covered with a thick external cuticle, and is maintained at high internal pressure. As a result, it is very difficult to access the neurons for study while maintaining the integrity of the circuit.

Early electrophysiological studies focused on neuromuscular function in the pharynx of the worm, using a suction electrode to record compound extracellular potentials termed electropharyngeograms (Raizen & Avery, 1994). A slit-worm preparation was devised to incorporate whole-cell patch-clamp techniques to record from *C. elegans* central neurons (Goodman et al., 1998). This technique was modified to record synaptic activity at the neuromuscular junction (Richmond et al., 1999). These techniques, in combination with genetic and behavioral analyses, have allowed the elucidation of the role of various receptors and synaptic proteins (reviewed in (Francis et al., 2003)). Recording from *C. elegans* neurons, therefore, while not trivial, is possible. For the analysis of neuronal spatiotemporal response characteristics, it is an extremely attractive approach, as it provides a high-temporal-resolution picture of neuronal dynamics.

1.6 Functional versus Static connectivity maps

The existence of wiring diagrams reconstructed from electron microscope data are immensely useful. Analyzing these maps have helped to target specific cells and pathways for genetic and behavioral analyses, to identify motifs of connectivity (Milo et al., 2002, Reigl et al., 2004) and to correlate neuronal structure and function using wiring cost optimization (Chen et al., 2006). However, these efforts would be

considerably aided by the addition of high-resolution data on the real-time processing undertaken by these neurons. Information on the weights of connections, whether and how they change, and which neurons are recruited in any particular task and in what order would open up an enormous range of interesting questions. In order to understand the dynamic functional connectivity, an understanding of the mechanisms of transfer and gain control are called for. Electrophysiological analyses, and to some extent, calcium imaging of neural activity are the tools that are most appropriate to convert our static connectivity maps into functional ones, by allowing us to monitor neural activity over different timescales, and during behavior.

1.7 Outline of Thesis

This thesis describes an attempt to characterize transfer at *C. elegans* synapses by combining electrophysiological and optogenetic techniques, by expressing ChR2 in pre-synaptic neurons and using whole-cell patch clamp recording techniques to monitor the post-synaptic neuron. Our attempt is the first functional characterization of the dynamics at central synapses in the worm. We begin by describing a prominent thermosensory synapse, between the sensory neuron AFD and the interneuron AIY, in Chapter Two. We find that this synapse is excitatory, has low gain, and exhibits graded and tonic release. Chapter Three describes a further voltage-clamp characterization of the AFD-AIY synapse and additionally, describes native voltage activated currents in AFD, AIY and ASER, a chemosensory neuron. In Chapter Four, we describes our analyses of the chemosensory synapse between ASER and AIY. We find

the synaptic response to be weak and unreliable. Finally, in Chapter Five, we present our conclusions and ideas for future directions.

Chapter 2

Transfer at a thermosensory synapse in *C.elegans*

2.1 The AFD-AIY synapse and the circuit for thermotaxis

C.elegans combines several useful features as a model organism for neural circuit analysis: a compact nervous system, detailed anatomical data from electron microscopy (EM), and access to system analysis tools such as precise genetic manipulations, focal laser ablations of individual neurons, and real-time monitoring of neural activity using calcium imaging and electrophysiology. In addition, having a small nervous system does not preclude the worm from exhibiting a range of behaviors that can be described quantitatively (de Bono & Maricq, 2005, Hobert, 2003). One such behavior is thermotaxis. When placed on a temperature gradient, worms aggregate to the temperature at which they were cultivated (T_{cult}) and track isotherms as narrow as 0.05°C near it (Hedgecock & Russell, 1975). Worms can track isotherms near T_{cult} in the presence or absence of food (Luo et al., 2006), although accounts differ on

whether the memory of T_{cult} is feeding-state dependent (Mohri et al., 2005) or not (Chi et al., 2007). A preliminary circuit, including neurons AFD, AIY, AIZ and RIA, was mapped using laser ablations (Mori & Ohshima, 1995).

Figure 2.1A shows these neurons along with some of their other significant synaptic partners. AFD has been shown to be the primary thermosensory neuron (Kimura et al., 2004, Mori & Ohshima, 1995), and temperature is sensed through an as-yet-unidentified mechanism located at the end of its sensory neurite (Chung et al., 2006). AFD serves as a precise sensor: calcium imaging experiments show that above T_{cult}, AFD Ca^{2+} levels can reliably track sinusoidal temperature variations as small as 0.05°C with phase lag of less than an eighth of a cycle (Clark et al., 2006). It appears that AFD codes for changes in temperature above a set point; this response is bidirectional and adaptive (Clark et al., 2007). In addition, electrophysiological experiments show that increases in temperature over the set point produces large depolarizations in AFD, while cooling hyperpolarizes the cell to a smaller extent (Ramot et al., 2008). How is this information conveyed to the next stage of the circuit? This forms the basis of our study. Electron-microscope data (White et al., 1986) provide the experimental basis for synaptic connectivity (Chen et al., 2006), showing that interneuron AIY is the primary postsynaptic partner for AFD. AIY also receives synaptic input from the other known thermosensory neuron AWC (Biron et al., 2008, Kuhara et al., 2008), as well as sensory neurons AWA and AWB. Calcium imaging data from AIY show that it also turns 'on' above a temperature set point, and responds in phase with the temperature stimulus variations (Clark et al., 2006).

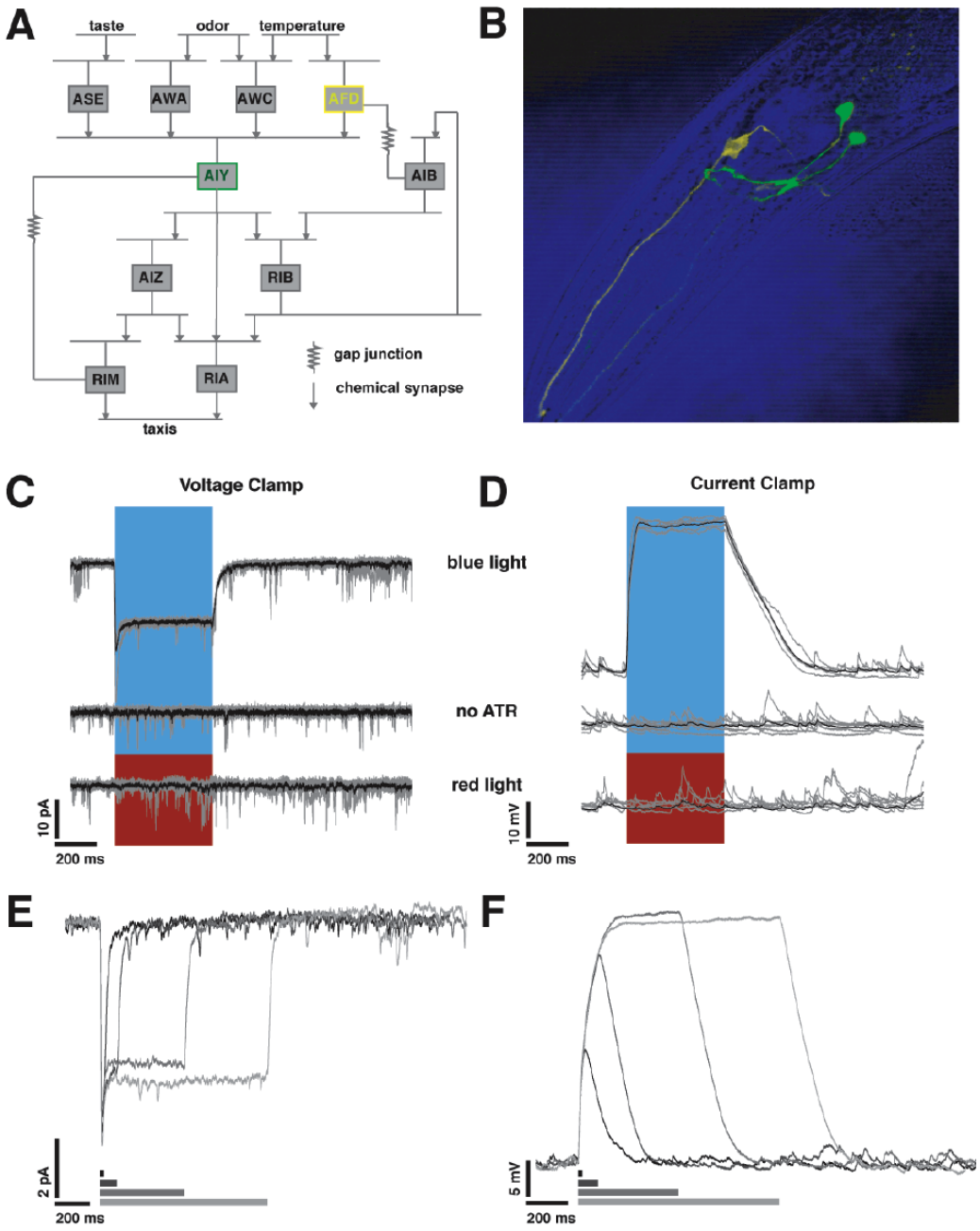

Figure 2.1: Using chR2 to stimulate AFD, the primary thermosensory neuron in C. elegans. A. Partial circuit diagram showing key cells involved in the thermosensory circuit and their synaptic partners. Adapted from (Mori et al., 2007). B. Confocal image showing AFD in yellow and AIY in green. There are two AFD neurons, left (L) and right (R). The second AFD neuron is fainter than the first owing to technical issues with obtaining the image. C. Voltage clamp recordings from AFD. A 500 ms pulse of blue light, and not red, causes inward current in AFD expressing functional chR2. All-*trans* retinal is required. 5 trials from a single neuron in gray, average in black. D. Current Clamp recordings from AFD in situations identical to (C). Light evoked depolarization in AFD can be controlled reversibly. Responses to 20, 100, 500 and 1000 ms light pulses in E. Voltage clamp and F. Current clamp.

Synaptic release from AFD has been examined using synaptopHlourin (Samuel et al., 2003). Those data, however, suggest that synaptic release from AFD occurs when $T>T_{cult}$ as well as when $T<T_{cult}$, a result inconsistent with Ca^{2+} imaging results that indicate that AFD calcium levels track changes in T above T_{cult} (Clark et al., 2006, Kimura et al., 2004). We note that while there are two AFD neurons, AFDL (AFD Left) and AFDR (AFD Right), electron microscope data show that they make symmetric connections to the pair of AIY neurons AIYL and AIYR. Additionally, no asymmetry has been observed in behavioral or ablation studies. Hence, here we adhere to established practice and refer to them collectively as AFD and AIY.

While our knowledge of the flow of information through the thermotactic circuit is significantly enhanced by these data, it would be useful to have a sensitive, high-temporal resolution picture of the synaptic activity at the AFD-AIY synapse, to begin to address questions of spatiotemporal integration, gain control, and transfer characteristics. Electrophysiology has been established in *C.elegans* (reviewed in (Francis et al., 2003)). We attempt to characterize transfer at the AFD-AIY synapse using established whole-cell electrophysiological recordings (Goodman et al., 1998, Hamill et al., 1981). Recording from both neurons simultaneously would be ideal but is currently not possible, given the size of the neurons (2-4 μm) and the short average duration of recording (tens of minutes). We thus looked to a recently developed technique of remote optical stimulation using channelrhodopsin-2 (chR2), a light activated cation channel (Boyden et al., 2005, Nagel et al., 2005, 2003). We limited expression of chR2, tagged with yellow fluorescent protein (YFP), to the presynaptic

neuron AFD, and visually identified postsynaptic neuron AIY for recording by the selective expression of green fluorescent protein (GFP) (Figure 2.1B). In addition to tracking the flow of information in the thermosensory circuit, this study will describe the basic features of synaptic transfer at a central chemical synapse in *C.elegans*.

2.2 Experimental Procedures

2.2.1 Strains

To identify AFD and AIY we used the strains PY1322 and OH98 expressing gfp in AFD and AIY respectively. We obtained the strain PY1322 *oyIs18 [gcy-8::gfp]* from the Caenorhabditis Genetics Center (CGC). OH98 (*mgIs32 [ttx-3::gfp, lin-15(+)];him-5*) was a gift from Oliver Hobert; we outcrossed it to N2 (wildtype) to eliminate the *him-5* mutation. We obtained the strain OH3192 (*ntIs1 [gcy-5::gfp]*) from the CGC and used it to identify ASER. We performed recordings on synaptic transmission mutants deficient in *unc-13*, a syntaxin binding protein, using the strain BC168 *unc-13(s69)* which was a gift from Anne Hart. We constructed a strain expressing chR2 in AFD, PS5755 (*syIs218 [gcy-8::chR2::yfp, pax-2::gfp, lin-15(+)]*), by injecting *gcy-8::chR2::yfp* plasmid DNA into MT1642 *lin-15(n765ts)* worms with the co-injection marker pHC294.1, a *pax-2::gfp* plasmid with GFP expression in the vulva and tail (a gift from Helen Chamberlin). We integrated the line by subjecting it to X-ray irradiation and out-crossing four times.

2.2.2 Molecular Biology

PCR was used to amplify the 2.258 kb fragment upstream of the *gcy-8* gene using the primers 5'-TCCCCCGGGATCTTGAGGACCTCGTCTTTAAGG-3' and 5'- CGCG-GATCC TTTGATGTGGAAAAGGTAGAATCGAAAATCC-3', and cloned into the Pml1 and BamH1 sites of the *Pmyo-3::ChR2(H134R)::YFP* plasmid (a gift from Alexander Gottschalk).

2.2.3 Experimental Setup

Worms were maintained in well-fed conditions at 20°C. Adults were prepared for experiments using established techniques (Goodman et al., 1998). Worms were prepared for chR2 experiments by feeding them all-*trans* retinal using existing protocols (Nagel et al., 2005).

Recipes for saline are as follows. Internal buffer: 143 mM KAsp, 0.1 mM CaCl2, 1.1 mM EGTA, 10 mM HEPES, 15 μM Sulforhodamine, 4 mM MgATP, 0.5 mM Na3GTP, pH 7.2, osmolarity 310 mOsm. Cs^{2+} and NMG^{+} solutions were made by substituting those ions for K^{+}. External buffer: 145 mM NaCl, 5 mM KCl, 5 mM MgCl2, 1 mM CaCl2, 10 mM HEPES, pH 7.2, osmolarity $\sim$ 320 mOsm.

Patch electrodes were pulled and pressure polished as described previously (Goodman & Lockery, 2000), for a tip resistance of 5-15 MΩ. Recordings were not corrected for junction potential and series resistance.

A small amount of negative current (mean: -5.46 pA, median -4.86 pA, interquartile distance -2.59 pA, n=66 cells) was injected into the neuron in current clamp to

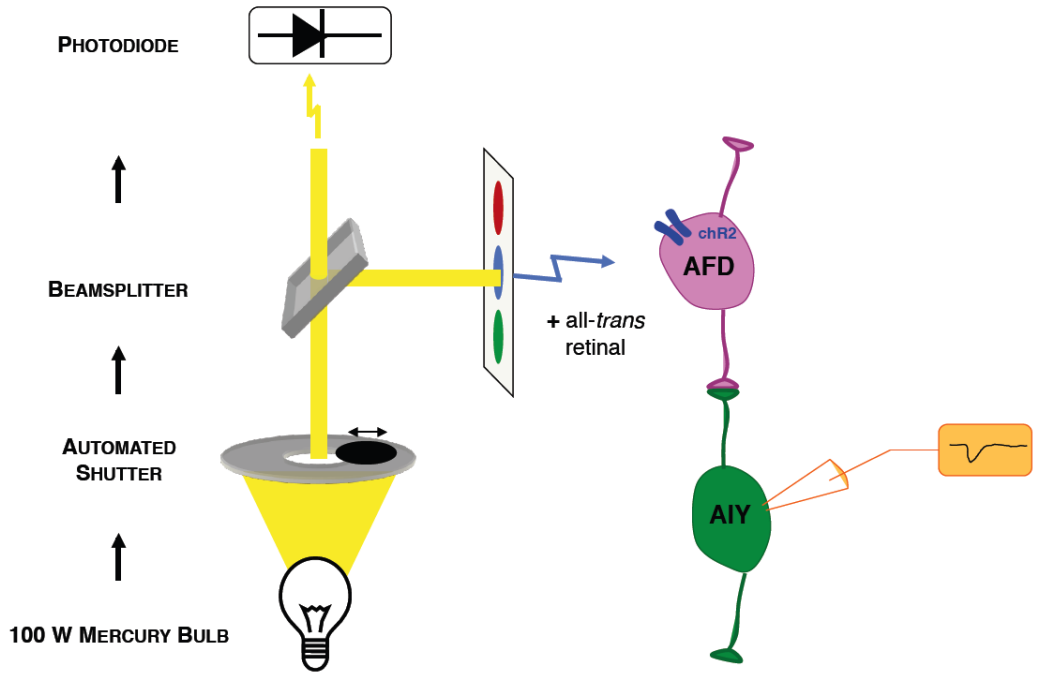

Figure 2.2: chR2 stimulation and recording setup. A 100W Mercury lamp provides light. A computerized shutter controls the shape of the light pulse. A beamsplitter sends a fraction of the light to a photodiode for real-time monitoring of the light stimulus, and the bulk of the light through a gfp filter to excite the preparation with blue light.

achieve a holding potential of around -65 mV (mean: -67 mV, median -66.8 mV, interquartile distance 3 mV, n=66 cells).

Light stimulus was provided using a 100W mercury lamp. A Sutter SmartShutter was used to control timing. The opening and closing latencies of the shutter were 8-12 ms. A liquid light guide was used to make the field of view uniform. The light was filtered using an Olympus gfp filter cube to provide blue light within the 450-490nm wavelength range. A high-speed silicon photodetector (Det100A, Thor Labs) was mounted on a beam splitter at the light source to continuously monitor the light stimulus waveform. Figure 2.2 shows a schematic of the setup. The peak intensity of light at the preparation was 348.5 μW/mm^2.

Data were acquired at 15 kHz using the Patchmaster program and a HEKA EPC-10 patch clamp amplifier, and filtered at 3 kHz. Analysis was performed using MATLAB.

2.3 Results

2.3.1 Light-evoked response in AFD

To depolarize AFD selectively and remotely, we expressed chR2 under the *gcy-8* promoter, which is exclusively expressed in AFDL and AFDR (Figure 2.1B). Worms were fed the co-factor all-*trans* retinal (ATR), necessary for functional chR2. To assess light-evoked control of AFD membrane potential, we first patched onto AFD and measured current and voltage changes evoked by light in that neuron. Doing these experiments in current clamp allowed us to estimate the kinetics and amplitude of a chR2-mediated potential in an unclamped neuron. In voltage clamp, we were able to evaluate chR2-mediated currents independent of other voltage-dependent currents. Using blue light, we could evoke inward currents of up to 10 pA and depolarizations of up to 40 mV (Figure 2.1C-D, topmost traces). Control experiments with worms fed no ATR (n=5) or using red light (n=7), showed no evoked potentials or currents (Figure 2.1C-D, middle and bottom traces). We could control AFD membrane current and potential reversibly for the duration of the light pulse (Figure 2.1E-F).

We computed rise and decay times and half widths for a dataset of 9 AFD cells subjected to a 500 ms light pulse. Mean 10-90% rise time (time for membrane po-

tential to go from 10% to 90% of steady state at maximal intensity) was 118.8 ms (median 121.3 ms, interquartile distance, iqr, 56.2). The decay of both the evoked current and potential could be fit with a single exponential function. The mean decay time constant of a voltage response to a 500 ms light pulse was 186.8 ms (median 145.3 ms, iqr 121.6 ms). The half-width (width at $\frac{1}{2}$ steady-state amplitude) of a voltage response to a 500 ms light pulse was 572.1 ms (median 552.5 ms, iqr 45.4 ms). For a light pulse of constant intensity 348.5 μW/mm^2, the amplitude at steady state of the evoked depolarization varied from 20 to 40 mV, with an average value of 28.2 mV (median 28 mV, iqr 9.7 mV, n =24). A similar range was observed in the evoked current (mean amplitude 11.35 pA, median 10.17 pA, interquartile range 8.1 pA, n = 21). This two-fold variability can probably be accounted for by the following three observations. First, chR2 expression likely varied across animals. Although the strain was constructed using an extra-chromosomal array integrated into the chromosome, we do not know the level of expression of the transgene in each animal. This is partly reflected in the observed variation in intensity of the YFP tag on the chR2 protein. Second, slight differences in AFD input resistance (mean 3.99 GΩ, median 2.58 GΩ, iqr 2.3 GΩ, n = 28), pipette resistance, and recording quality were unavoidable. Third, the amount of all-trans-retinal taken up by the worm likely varied across individuals.

We varied the intensity of our light stimulation over five orders of magnitude and measured the corresponding AFD depolarization. Figure 2.3A shows an example recording from AFD, in response to 500 ms light pulses of varying light intensity.

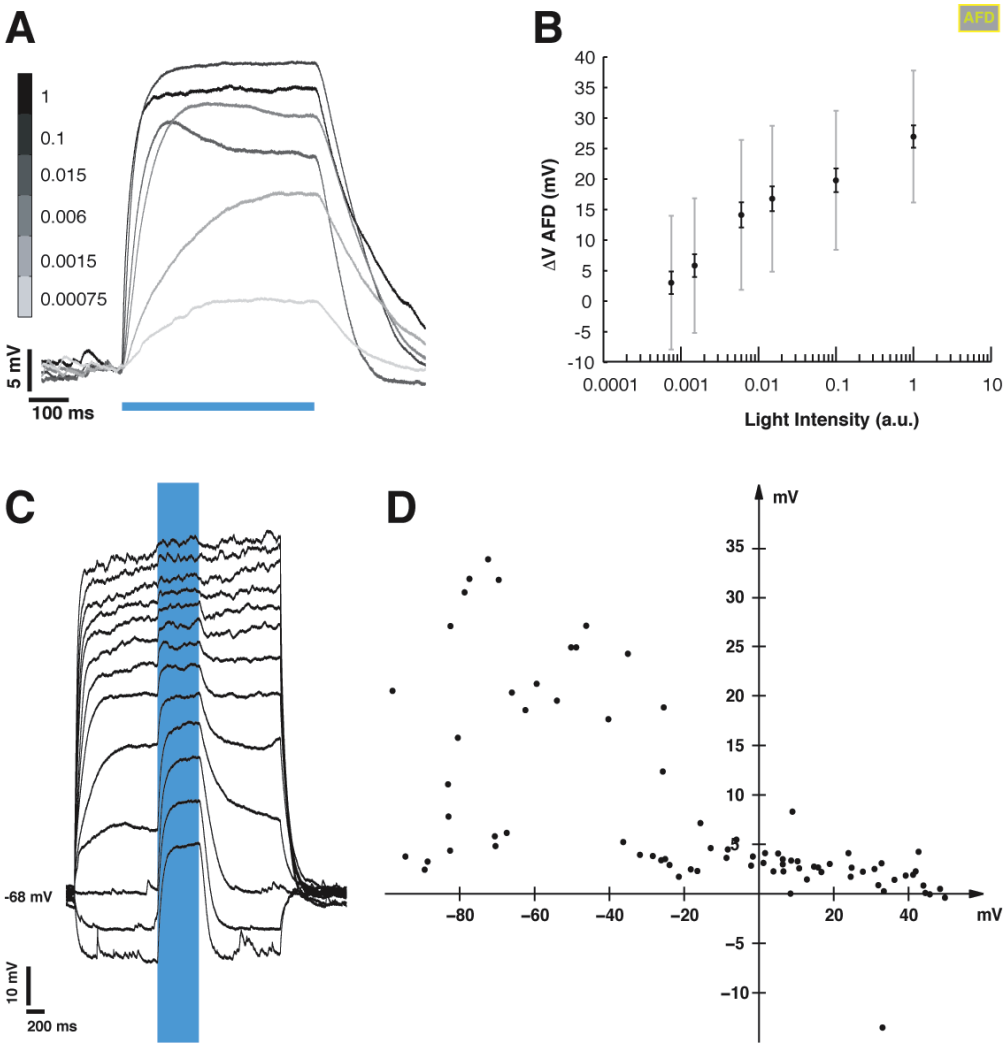

Figure 2.3: Calibrating AFD response to Blue Light. A. Depolarization evoked in AFD in response to 5 orders of magnitude variation in light intensity, 10-trial averages from example neuron. B. Average evoked depolarization in AFD as a function of normalized light intensity (gray bars ±SD, black bars ±SEM). C. Depolarization evoked in AFD as a function of holding potential, example recording. D. Evoked potential as a function of holding potential, pooled data.

Membrane potential varied log-linearly with light intensity (Figure 2.3B, n=7).

A variety of resting potentials, ranging from -30 mV to -70 mV, have been described for non-spiking cells with graded synapses (reviewed in (Siegler, 1984)). Typically, these cells tend to be more depolarized than spiking neurons. It is important to take this into account, since the value of resting potential that we attempt to mimic with our holding potential will affect our transfer function, as the membrane may have different regimes of behavior varying with potential. In the absence of true estimates of resting potential, we attempted to assess the effect of holding potential by injecting current to clamp AFD at different voltage values and assessing the evoked depolarization. We clamped the cell from +40 mV to -100 mV and measured the response to a fixed light pulse at each step. We note that the light evoked depolarization in AFD varies as a function of holding potential (Figure 2.3C shows an example set of traces from one neuron, the V-V curve in Figure 2.3D shows the variation of evoked potential with holding potential, 7 trials from 6 neurons), and over the range of -30 to -70 mV, the evoked depolarization is in the range of 20-40 mV. This is comparable to the depolarization we evoke in our experiments with a holding potential of $\sim$-65 mV.

2.3.2 Depolarization of AIY by presynaptic, light-evoked depolarization

Having established a calibration of our presynaptic light-evoked depolarization, we next stimulated AFD with light and recorded from AIY. Upon brief (20 ms, 348.5

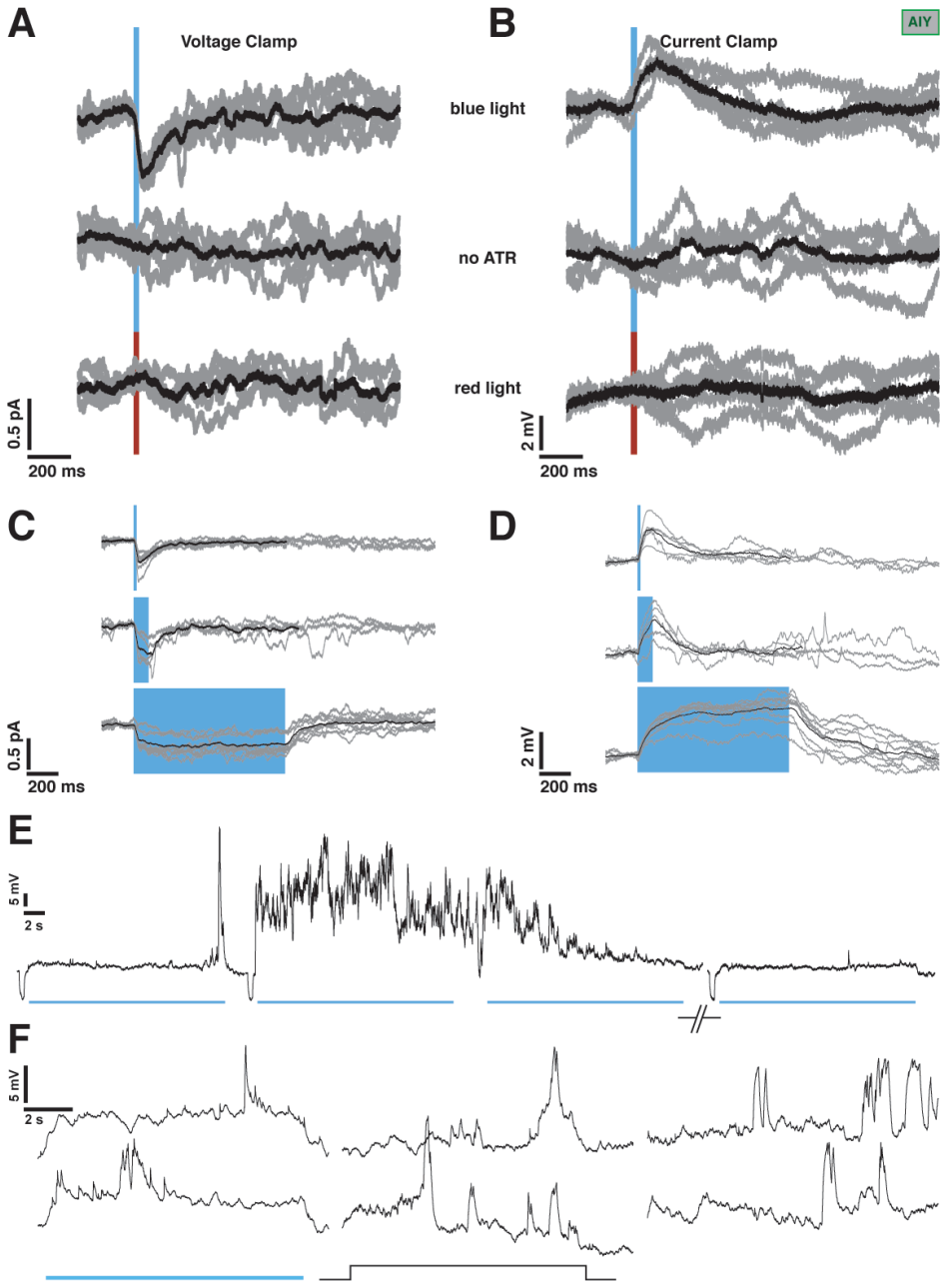

Figure 2.4: Synaptic Response in AIY is tonic. A 20 ms pulse of blue light is sufficient to evoke synaptic response in AIY in A. Voltage clamp and B. Current clamp. Controls show no response. Response of AIY is tonic (20, 100, 1000 ms light pulses) both in C. Voltage clamp and D. Current clamp. 5-trial averages of individual neurons in gray, average of all cells in black. E. AIY responses to long pulses of light. Four trials of AIY response to 20 s blue light. Each trial is preceded by a small hyperpolarizing pulse to measure input resistance. F. Example traces of AIY response to 10 s of blue light (left, two trials), 10 s of 100 fA current injection (middle) and 10 s of no stimulus (right). In all cases the neurons were held $\sim$ -65 mV.

μW/mm2) light stimulation, we recorded postsynaptic currents and potentials (pscs and psps) of 0.5 pA and 3-5 mV respectively (Figure 2.4A and B). The profiles of these synaptic responses were reminiscent of classical, spike-mediated (Fatt & Katz, 1951) or epsp-mediated (Burrows, 1979) pscs and psps recorded in other systems. Controls with worms fed no ATR (n=2) or with presynaptic stimulation with red light (n=8) showed no evoked responses (Figure 2.4, middle and bottom traces).

Because each AFD neuron (L and R) contacts both AIY neurons (8-12 points of synaptic contact (Chen et al., 2006), the current and voltage recorded in one AIY neuron must have always been responses to the aggregate synaptic input from two AFD neurons. The peak synaptic currents were small (mean -0.69 pA, median -0.60 pA, iqr 0.37 pA, n=28). This is consistent with the small depolarizations (mean 2.1 mV, median 2.3 m, iqr .82 mV, n= 17) we recorded in current-clamp (AIY mean input resistance 5.9 GΩ, median 5.47 GΩ, iqr 1.25 GΩ, n=38). Other than the possibility that the weight of this synapse is intrinsically low, such small size may result from some other considerations. The first possibility is that much of the synaptic current was shunted away from the recording site, the cell body, by the interposed neurite. This view is consistent with Ca^{2+} imaging results in which no significant changes in Ca^{2+} signal could be observed at the cell body of AIY. Instead, measurements were made at a point along the neurite where it bends into the nerve ring (Chalasani et al., 2007, Clark et al., 2006). The second possibility is that voltage-clamp was imperfect, leading to unclamped outward conductances evoked by the psp's depolarization. To test this hypothesis, we substituted Cs^+ for K^+ in our pipette (n=8; see Section 3.2).

In half of the recordings, this abolished the synaptic response; in the other half, there was no decrease in the evoked current. This result is perplexing, and there could be several factors at work here. It is possible that the synapses were ruptured in some of our recordings. However, since we visually ensure the integrity of the neurite before commencing recording, this is unlikely, and certainly unusual if it were to be the case in half of our recordings. Alternatively, while the profile of voltage-activated currents were similar in neurons with and without synaptic responses, indicating that Cs^+ was effective in the soma, it could be that in some recordings, Cs^+ was not adequately delivered to the synaptic site. Overall, we cannot conclude substantively whether Cs^+ affected the synaptic response.

As a point of comparison, we analyzed spontaneous events occurring in AFD (see Figure 2.1C baseline for examples, also Figure 2.5C). The frequency of very similar events (Figure 2.5A-B, rightmost four panels) in another amphid cell ASER was dramatically reduced in an *unc-13* background (Figure 2.5B; wild type (wt), 740 events from 4 neurons; *s69* (an allele of *unc-13*), 357 events from 3 neurons). A mutation in *unc-13*, a syntaxin binding protein, reduces synaptic transmission dramatically, and the fact that the spontaneous events were reduced in *unc-13* animals suggests that these events were synaptic in origin. The frequency of such events in AFD itself was not reduced in an *unc-13* background (Figure 2.5A; wt, 731 events from 7 neurons; *s69*, 521 events from 3 neurons). In AFD, the spontaneous events were around 2 mV in amplitude (mean 2.3 mV, median 2 mV, iqr 1.5 mV) with low rise times (mean 5.6 ms, median 5.1 ms, iqr 4.4 ms) and slow decay times (mean 18.3

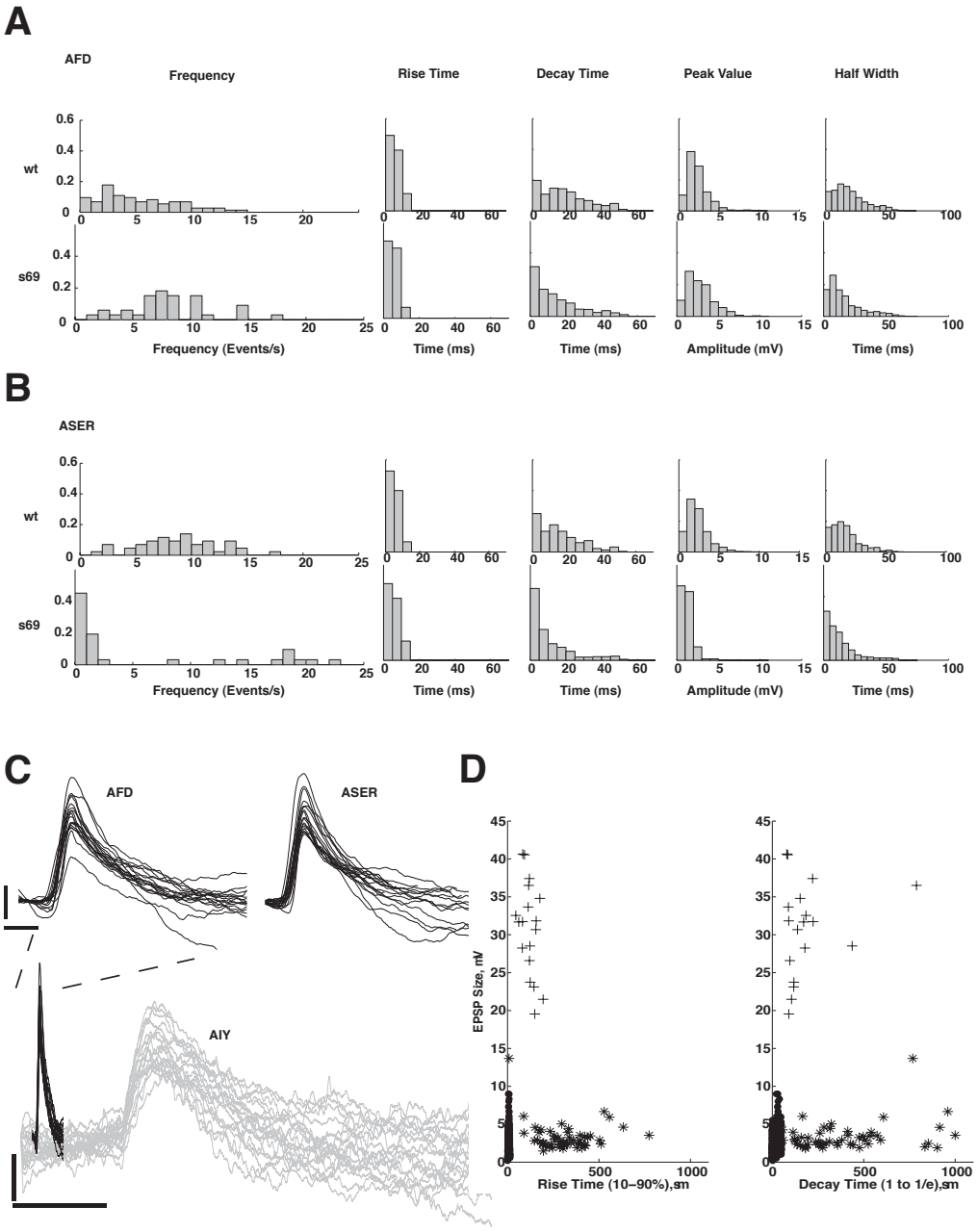

Figure 2.5: Spontaneous events in AFD and ASER. A. Analysis of spontaneous events in AFD. Histograms for wild type (*wt*), top row,and *unc-13(s69)*, bottom row. B. Spontaneous events in ASER. Histograms, top row -*wt*, bottom - *unc-13(s69)*. C. Example traces of spontaneous events in AFD (top left) and ASER (top right) and AIY (bottom). The AFD examples are replotted on the same scale as the AIY traces for ease of comparison. Scale bar, top: 1 mV, 10 ms. Scale bar, bottom: 1 mV, 200 ms. D. Scatter plots of rise and decay times for AFD 500 ms depolarization (+), AFD spontaneous events (.), and AIY synaptic response to 500 ms pulse (*).

ms, median 17 ms, iqr 18.8 ms; Figure 2.5A). It could be that in AFD, the events are non-synaptic in origin, although their kinetics are remarkably similar to those in ASER (see Figure 2.5A-C).

The rise and decay times for the AIY synaptic response differed from those of the events in AFD by more than an order of magnitude. In response to a 20 ms blue light pulse, the mean 10-90% rise time was 131.6 ms, with median 104 ms and iqr 166.6 ms (n=9) and decay was 659.3 ms mean (median 638.0 ms, iqr 339.8 ms, n=9). For a light pulse of 500 ms, the rise times were longer (mean 310 ms, median 304 ms, iqr 43.2 ms; n=6) although decay times were shorter (mean 384.2 ms, median 363.2 ms, iqr 160.4 ms; n=6). Since the overall depolarization resulting from a 500 ms pulse is larger, it could be that the membrane voltage takes longer to peak; the recruitment of voltage dependent conductances could shorten the decay times. In total, these data suggest that the mechanisms underlying the AIY response are very different from those underlying the events in AFD and ASER.

The excitatory synaptic potentials (epsps) that we measured from AFD to AIY must be multivesicular, since, as mentioned earlier, we measure aggregate synaptic activity onto AIY from AFD. This usually implies larger epsps and a wide range of decay times (if release is asynchronous). However, if the event underlying release is a quick depolarization (say the rising phase of the presynaptic depolarization event) then release need not be asynchronous. We see a wide distribution of decay times, consistent with asynchronous release, albeit a fairly narrow range of sizes (Figure 2.5D).

2.3.3 Release at the AFD-AIY synapse is tonic

We stimulated AFD with light pulses of varying duration. Figure 2.4 C-D show evoked currents and potentials in AIY for three different pulse durations: 20 ms, 100 ms, and 1 s. Longer pulses (10 s; Figure 2.4F, leftmost two traces) and up to 20 s (Figure 2.4E) indicated a sustained component to the response lasting as long as the presynaptic depolarization. In addition, the membrane of AIY displayed rich dynamics: we observed both depolarizing and repolarizing transients ranging in size from 5-25 mV. These transients were observable in the presence of blue light, with a 100 fA current injection, and while holding the neuron close to presumed rest (Figure 2.4F).

2.3.4 Release at the AFD-AIY synapse is graded

We varied the intensity of our light stimulation over five orders of magnitude and measured the AIY synaptic response. We found that release at the AFD-AIY synapse is graded over the range sampled. Figure 2.6A shows an example recording from AIY. Each trace is a ten-trial average of membrane voltage in response to a 500 ms light pulse of varying light intensity. Membrane potential varied log-linearly with light intensity (Figure 2.6B, top; n=4). Having performed similar recordings from AFD (see Figure2.3), we could extract an estimate of the synaptic transfer function between AFD and AIY. This function is plotted in Figure 2.6B (bottom), with linear regression fit (regression coefficient=0.056, R2 = 0.69). This suggests an apparent gain of less than 0.1 mV of postsynaptic response for each mV of presynaptic depolarization

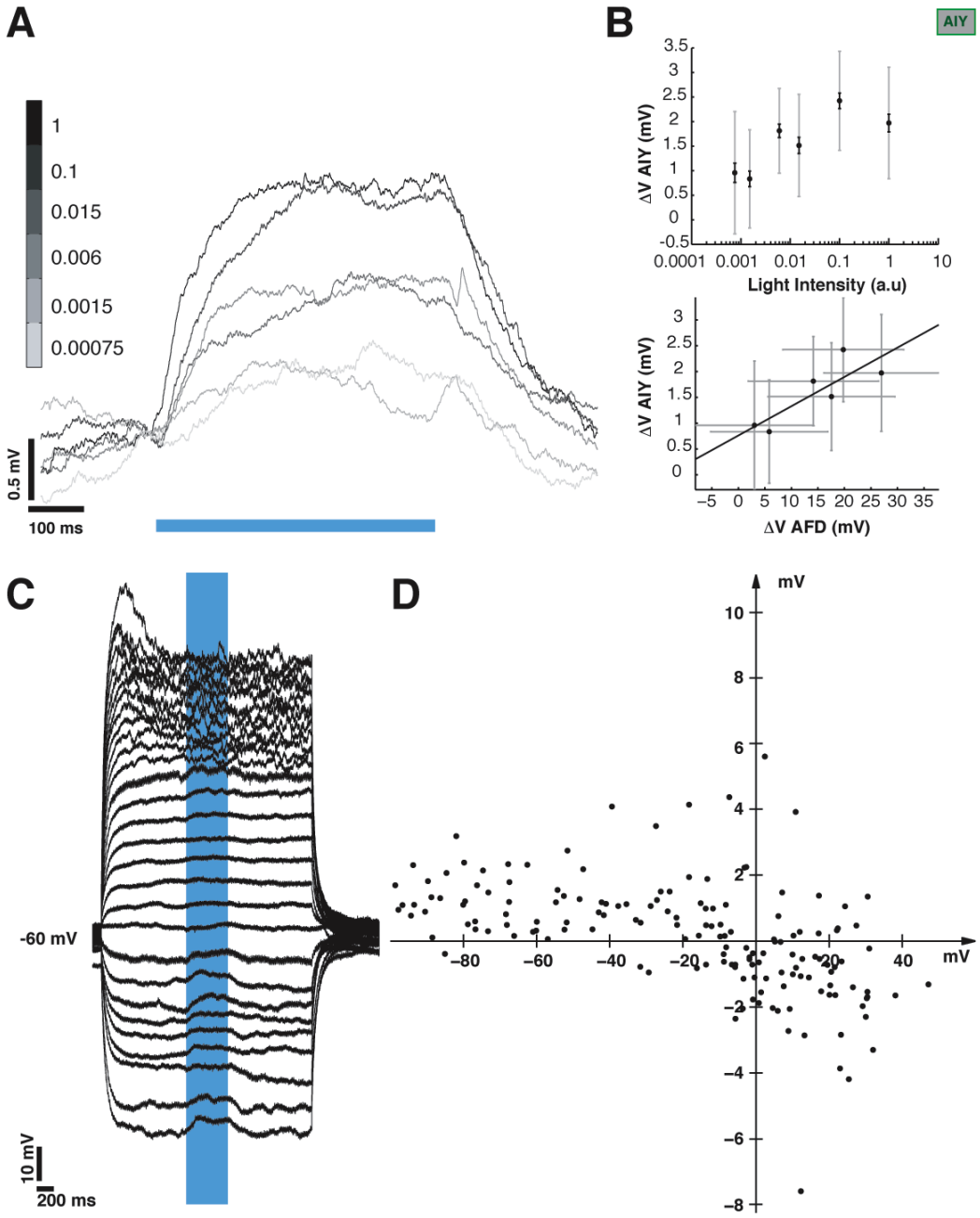

Figure 2.6: AIY synaptic response is graded and reverses between -20 mV and 0 mV. A. Depolarization evoked in AIY in response to 5 orders of magnitude variation in light intensity, 10-trial averages from example neuron. B. Top: Average evoked depolarization in AIY as a function of normalized light intensity (gray bars SD, black bars SEM). Bottom: Transfer function of the AFD-AIY synapse. Average evoked depolarization in AIY as a function of average evoked depolarization in AFD. (gray bars SD, R2 = 0.69). C. Reversing the AIY synaptic potential. Example recording, with AIY held at different potentials. D. Evoked synaptic depolarization as a function of holding potential, pooled data.

within the range explored.

2.3.5 The synaptic potential reverses between -20 and 0 mV

If the synapse between AFD and AIY is chemical, it must have an associated ionic conductance and thus, reversal potential. To assess the value of this putative reversal potential, we imposed a presynaptic light-evoked depolarization while AIY was held at holding potentials between -100 and +40 mV (Figure 2.6C; 7 trials from 4 neurons). The synaptic potential appears to reverse between -20 mV and 0 mV (Figure 2.6D). The synaptic depolarization becomes more pronounced at hyperpolarized potentials, although the amplitude variation was less dramatic. At more depolarized holding potentials, the membrane response became noisier. This is probably due to the opening of other voltage-activated conductances, which might explain the greater variability in evoked response size.

We attempted the same experiment in voltage clamp; however due to the small size of evoked currents it was difficult to resolve changes with holding potential. Data from those experiments are presented and discussed in Chapter 3.1.

2.3.6 No evidence of facilitation or depression at the AFD-AIY synapse: frequency independent

We stimulated the synapse with trains of pulses ranging in width and intervals from 20 ms to 1 s. We observed no significant change in the size of the synaptic response. Figure 2.7A shows an example trial each for AFD and AIY stimulated at 500 ms

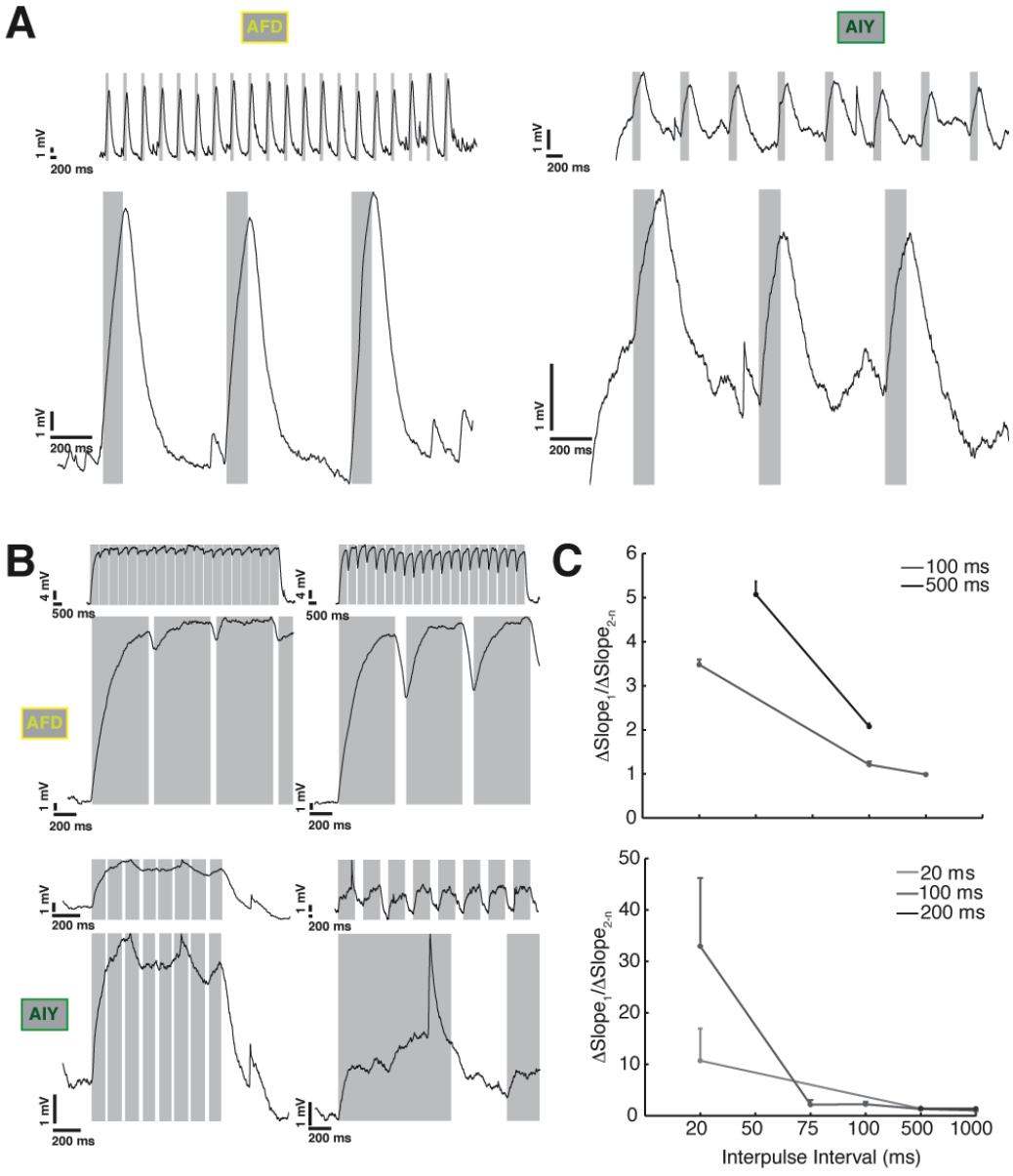

Figure 2.7: AFD and AIY response to different pulse stimulation protocols: no evidence for facilitation and depression. A. Example traces of AFD (left) and AIY (right) responses to light pulse trains (2s). Inset: entire sequence of pulses. [pulse width, interval] values: [100ms, 500ms]. B. More examples. AFD [pulse width, interval] values: left [500 ms, 50 ms], right [500ms, 100 ms]. AIY [pulse width, interval] values: left [100 ms, 20 ms], right [1000ms, 500 ms]. C. Frequency dependence of the ratio of the size of the first pulse to subsequent pulses in the train. Top, Variation in slope with pulse width and interval in AFD; Bottom, in AIY. Bars +SEM.

intervals with a pulse of length 100 ms. Figure 2.7B shows more examples. We calculated the ratio of the amplitude of the first evoked response to the average of the succeeding responses and compared these across different interpulse intensities; we found no clear trend. We also computed a similar metric: ratio of the slope of the rising phase of the first pulse to the average of the succeeding ones; here, we found a decreasing trend that was mirrored both pre and post-synaptically (Figure 2.7C). We conclude that there is no frequency dependence in the evoked potential, and no obvious facilitation or depression, at least within this range.

2.4 Discussion

Previous ablation and imaging studies show that the neuron AFD responds to warming (Kimura et al., 2004) and that it senses temperature at the distal end of its dendrite (Chung et al., 2006). Our stimulation of this synapse substitutes light-mediated ChR2 activity for temperature and, indeed, is the first study to do so. How relevant are our stimulation levels to those that AFD experiences in vivo? Electrophysiological data (Ramot et al., 2008) indicate that AFD responds to changes in ambient temperature with inward currents of $\sim$10 pA and depolarizations of $\sim$40 mV when $T > T_{cult}$. These values are comparable to our ChR2 mediated currents and voltages in AFD. With stimulation in this range, the present study shows that the AFD-AIY synapse is graded and tonic, with a faithful rendering of 'ΔT' from AFD to AIY.

The first graded central synapses to be characterized were in the metathoracic ganglion of the locust, between nonspiking local interneurons and motorneurons (Burrows

& Siegler, 1976, 1978); release at these synapses is tonic, and is generally hyperpolarizing. Central graded and tonic synapses have been described in other arthropod systems as well, such as in the insect retina (Juusola et al., 1996) and the crustacean stomatogastric ganglion (Graubard, 1978).

The characteristic feature of a graded synapse is that release is sustained and has low threshold. The input output curve for a spiking synapse is shifted to the right relative to that for a graded synapse (and requires abolishing spikes using TTX to reveal it). At a spiking synapse release is not a continuous function of membrane voltage - an action potential is required to trigger release. However, a lack of action potentials is not necessary for a neuron to possess a graded synapse. A spiking neuron can have both spike dependent and independent synapses - for example the L neuron in the locust ocellar visual system (Simmons, 1982) and spiking motor neurons in the stomatogastric ganglion of the lobster (Graubard et al., 1980).

In vertebrate graded synapses such as those in the retina and the cochlea, sustained release is typically correlated with the presence of organelles called ribbons (Sterling & Matthews, 2005), and fast replenishment of a large pool of vesicles (Griesinger et al., 2005). Spiking neurons do not appear to possess ribbons, yet fast reloading from a large releasable pool can sustain tonic release (Saviane & Silver, 2006). Central nonspiking synapses in the locust also do not posses ribbons (Watson & Burrows, 1988). Release at the AFD-AIY synaptic was frequency independent, showed no sign of short-term facilitation and depression in the range explored, and could be sustained for as long as 20 seconds (Figure 2.4E-F). Electron microscope data (White

et al., 1986) do not show evidence of the existence of ribbon synapses in C. elegans, but do indicate that there are multiple release sites between AFD and AIY (Chen et al., 2006). Multiple release sites might be a partial explanation; in addition, the sustained release could imply the existence of large presynaptic vesicle reserves or fast replenishment mechanisms.

The identity of the neurotransmitter at the AFD-AIY synapse is unknown. AFD is known to produce several neuropeptides (Colosimo et al., 2004), and thermotaxis is known to have a glutamate- mediated component: worms carrying a mutation in the vesicular glutamate transporter *eat-4* show a weakened cryophilic response above T_{cult} (Clark et al., 2007). AIY expresses a putative metabotropic glutamate receptor (Wenick & Hobert, 2004); and RIA, an interneuron downstream of AIY, exclusively expresses the *glr-3* encoded kainate receptor (Brockie et al., 2001). There has also been speculation on the sign of the signal transmitted from AFD to AIY (Chung et al., 2006, Mori & Ohshima, 1995). Our experiments establish that the transfer between AFD and AIY is excitatory, with an apparent reversal potential between -20 mV and 0 mV, consistent with a mixed cationic conductance. A characterization of the neurotransmitter(s) and receptor(s) mediating the response will have to await detailed pharmacological tests.

Do our results exclude the possibility that there exists an electrical synapse between AFD and AIY? Existing electron microscope data provide evidence for chemical synapses and not gap junctions between AFD and AIY, although the latter could well still exist and have been missed. The fact that the AIY response depends on holding

potential implies that it is, at least in part, a conductance mediated synapse.

Transmitter release at graded synapses is usually not only sustained, but also activated at low presynaptic voltages. Consequently, depolarization as well as hyperpolarization of the presynaptic neuron can cause modulations of transmitter release and thus, postsynaptic responses (Burrows & Siegler, 1976). Previous work suggests that AFD is capable of resetting its membrane voltage based on temperature changes in either direction (Ramot et al., 2008). Whether this modulates neurotransmitter release in vivo depends on the overlap between the normal dynamic range of the presynaptic voltage and that of release at the synapse. If AFD spends significant amounts of time in the voltage range where release occurs, then AIY would experience variations of potentials in both polarities following AFDs voltage fluctuations. In C. elegans, we do not yet know the true resting potential and range of voltage variations of AFD in vivo. Our estimates of true pre- and postsynaptic membrane potentials were also likely inaccurate, for our recordings were always made from the soma, electrotonically distant from the presumed sites of release. Multiple research groups have been unable to record significant Ca^{2+} transients at the AIY cell body, monitoring instead a spot further along the neurite where stimulus-evoked changes in Ca^{2+} can be measured (Chalasani et al., 2007, Clark et al., 2006). This observation, along with the small size of our evoked current and filtered shape of our recorded potential suggests that the electrical signal may be shunted away from the cell body by the neurite. The fact that we were unable to completely reverse the synaptic potential in AIY even though we subjected the neuron to a wide range of holding

potentials, lends credence to this hypothesis. Of course, there are a number of other possible reasons for incomplete reversal: first, we could be activating large outward conductances by clamping the cell at large positive values of membrane potentials. Similar experiments in voltage clamp show a variety of inward and outward currents that activate at depolarized values (data not shown). Second, the response at AIY could be due to a highly rectifying channel. Strongly rectifying synapses exist; for example, the graded synapse between rod-horizontal cells in tiger salamander retina clips the signal above a certain amplitude (Attwell et al., 1987). Third, we could be inadequately clamping the synapse due to improper space clamp, in which case our clamp voltage would have limited effect. Much thus remains to be done to fully understand transfer at this synapse.

Sustained release can last for several minutes - at least 5 minutes between locust ocellar L neurons and third order neurons (Simmons, 1981), or, in cases where the resting membrane potential is depolarized above neurotransmitter release threshold, possibly indefinitely: for example, the locust L neurons (Simmons, 1981), and non spiking neurons in locust thoracic ganglia (Burrows & Siegler, 1978). Other graded synapses such as the EX1-GM synapse in the lobsters stomatogastric ganglion (Graubard, 1978) show evidence of multicomponent (early peak followed by lower plateau) postsynaptic responses, which might involve presynaptic conductance changes and/or postsynaptic desensitization. We observed no such multicomponent responses at the AFD-AIY synapse. We observed, however, declining postsynaptic responses with long (>=10s) light-induced presynaptic depolarization, consistent with

desensitization.

We could characterize transfer at the AFD-AIY synapse only in its linear range; technical and biophysical constraints prevented us from measuring threshold and saturation. As in other synapses (lobster stomatogastric ganglion (Graubard, 1978), lamprey (Martin & Ringham, 1975) and the squid (Kusano, 1968)) this range of the input-output curve allowed us to estimate its peak (apparent) gain: gain at the AFD-AIY synapse was low (around 0.1). Gain factors of <1 are not uncommon: at locust nonspiking synapses, such as that between the ocellar L neuron and a 3rd order neuron, transfer gain is 0.5 (Simmons, 1981), or 1 (Simmons, 1993). This low gain seems consistent with the fact that the L neuron integrates information from multiple sources (Simmons, 1999). High-gain synapses imply high sensitivity and high signal-to-noise ratio; they must, however, be paired with some form of adaptation so as to maintain a large operating range. Synapses from photoreceptors typically fall into this category: for example, the blowfly photoreceptor synapses have a gain of 6 (Laughlin et al., 1987), while locust ocellar synapses have a gain of 20 (Simmons, 1995). Compressing a highly dynamical signal into a smaller range would ensure that AIY, receiving input from multiple channels, is not saturated by any one input stream.

At spiking synapses, presynaptic Ca^{2+}entry is maximum during the tail current (during the repolarizing phase of the spike), where the driving force on Ca^{2+} is greatest (Llinas et al., 1981). If the presynaptic depolarization in AFD was faster and transient, the tail current would be larger, and the gain of the synapse could be

higher. In general, non spiking synapses tend to be slower, and presynaptic Ca currents typically tend to be carried by L type Ca^{2+} channels at graded synapses, as opposed to P- and N-type channels at spiking synapses (Juusola et al., 1996). Such channels exist in the C. elegans genome, and at least one of them, *egl-19*, is expressed in AFD (Erich Schwarz, personal communication).

What do our results imply for the functional and computational role of this synapse? The fact that the AIY response is tonic, shows no adaptation and is frequency independent over the range of inputs explored would suggest that the role of this synapse is to provide AIY with a faithful scaled- down version of temperature changes tracked by AFD. The low gain at this synapse is also consistent with the presumed integrative role AIY plays as it processes multiple streams of sensory information. In our results, AIY responses are graded, but the range is fairly compressed. This implies that AIY may not make the most of the analog information encoded in the amplitude of the synaptic input from AFD. In principle, graded synapses can encode information using both timing and amplitude variables. Amplitude coding is used to limited effect in some cases, however. One such example is the synapse between nonspiking neurons 151 and mechanosensory P neurons in the leech (Marin-Burgin & Szczupak, 2000) where the maximum amplitude of the synaptic potential is similar over the range of behaviorally relevant input frequencies, and the information appears to be coded primarily using the duration of the depolarization and the time to reach the maximum amplitude. Nonspiking local interneurons in the locust implement an adaptive gain control mechanism through the matching of synaptic and

membrane nonlinearities (Laurent, 1993). This gain control has the effect of linearizing polysynaptic pathways, and presenting information to downstream neurons in a context-independent way. Such mechanisms, if employed at the AFD- AIY synapse, would allow it to isolate and process thermosensory information in a separate channel, ensuring a reliable and accurate representation of the thermal environment.

ChR2 has been used as a tool to study synaptic transfer at the C. elegans neuromuscular junction (Liewald et al., 2008, Liu et al., 2009). Our study is the first characterization of a central synapse in *C. elegans* using this method. Taken together, these studies establish the use of ChR2 as an effective tool in the analysis of the neural circuitry of the worm.

Our ChR2-mediated presynaptic stimulus (ranging from 20-40 mV at the soma) evoked, at most, a response of 2-4 mV in AIY. In the absence of obvious integration of AFD input over time, does this represent an upper bound on the input that AIY receives from AFD? It is not known if depolarizing psps from AFD to AIY alone are adequate to trigger thermotaxis. We sometimes observed large depolarizing transients (20-30 mV in amplitude) at the AIY soma (see Figure 2.4E-F). This observation raises several interesting questions regarding the processing further downstream, such as what causes AIY to release neurotransmitter in turn, how it integrates information from AFD with signals coming in from other chemosensory neurons, and whether it needs conjunctive input from other neurons or long range neuromodulatory influences to be activated.

The present study employs remote optical stimulation of a targeted central synapse

in C. elegans and shows that the transfer at the AFD-AIY synapse is excitatory, graded, tonic, and reliable over tens of seconds. This synapse appears to be well suited to transmitting temperature difference information encoded in AFD to AIY, showing a response that is time- and frequency- invariant; the low (<0.1) gain may facilitate processing in AIY by rescaling its input to stay within its dynamic range. The use of optical stimulation techniques in combination with physiology can serve as a powerful tool in our efforts to understand how this compact nervous system processes information to shape a worm's response to its environment.

Chapter 3

Further characterization of synaptic and native currents in AFD, AIY and ASER

In the previous chapter, we characterized the first synapse in the thermosensory pathway in *C. elegans*. The synapse was graded and tonic with low gain. The evoked currents and potentials were small (<0.5 pA and ∼2-4 mV). In this chapter, we describe additional features of the synaptic response, and provide a preliminary characterization of the native voltage-dependent currents exhibited in AIY. In addition, we document the spontaneous psps we recorded from a variety of neurons.

3.1 Reversal of the AFD-mediated synaptic current in AIY

We previously characterized the synaptic potential evoked in AIY in response to stimulating the presynaptic neuron AFD with blue light (see Figure 2.6C). Additionally, we attempted to reverse the synaptic current (Figure 3.1A). We explored a wide range

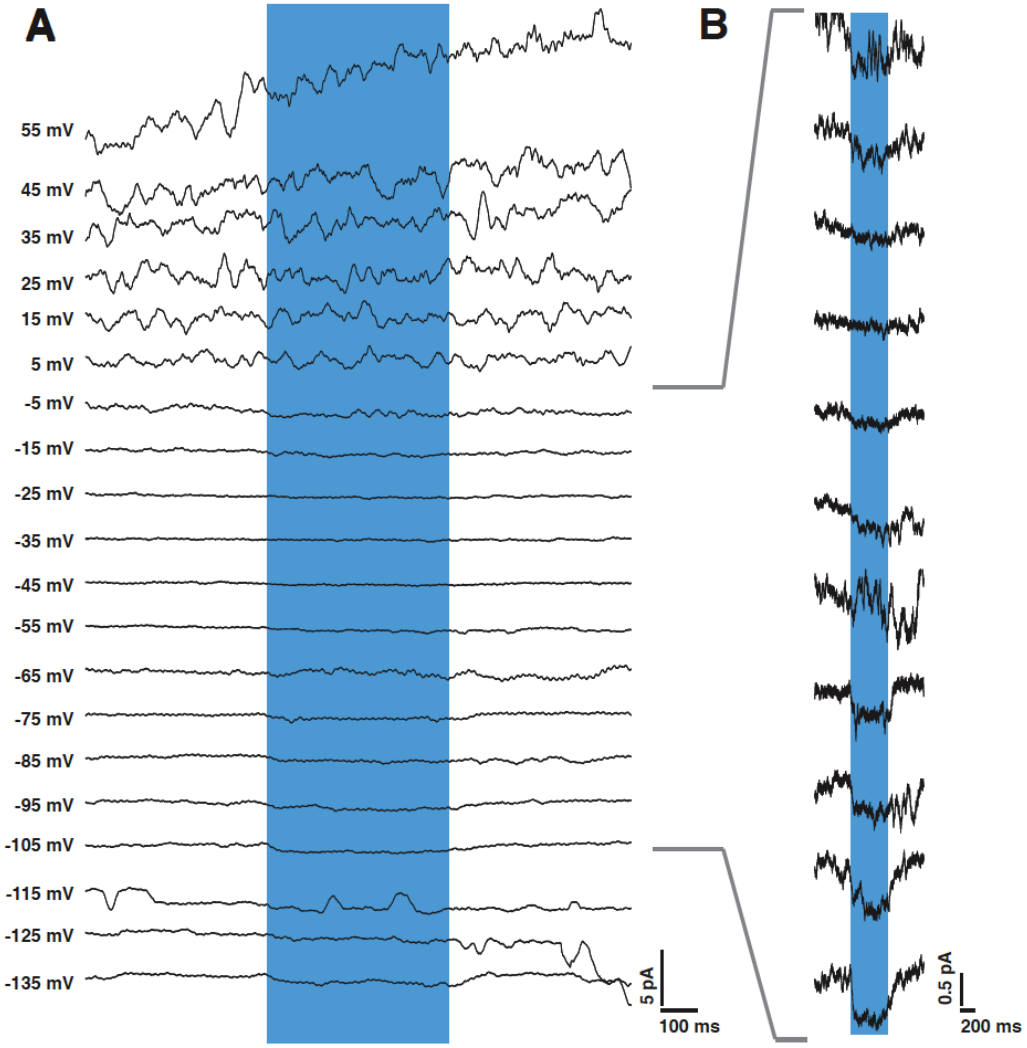

Figure 3.1: Reversing the AFD-mediated synaptic current in AIY. A. Synaptic current evoked in AIY in response to a 500 ms pulse of blue light while holding the neuron at potentials ranging from +55 mV to -115 mV. B. A closer look at the small but distinct currents evoked at potentials ranging from -5 mV to -105 mV

of holding potentials. As the potential became more depolarized, the synaptic current grew smaller in size (Figure 3.1B). As the membrane was depolarized beyond zero, other voltage activated currents came into play (described in more detail in Section 3.3), and it was difficult to isolate the synaptic current. On average, the evoked synaptic current was very small, on the order of 0.5 pA, and it is not surprising that it is masked by other larger voltage activated currents. An estimate of the reversal potential can be obtained from the I-V curve (Figure 3.2). The current appears to reverse in the neighborhood of -20 mV to 0 mV, which is consisted with a mixed-cationic current. The data are also in agreement with current clamp data estimating the reversal of the synaptic potential in the same neighborhood (see Figure 2.6D).

3.2 Effect of Cs^+ on the AFD-mediated synaptic current

As noted earlier, our observed synaptic responses were distinct, yet small. There could be a variety of reasons for this, as discussed in the preceding chapter (see Section 2.3.2 and Section 2.4). In order to eliminate unclamped or unrelated outward conductances, we substituted Cs^+ for K^+ in our pipette (n=8, Figure 3.3A). In half of the recordings, this abolished the synaptic response; in the other half, there was no decrease in the evoked current (Figure 3.3B). As discussed in the preceding chapter, there are at least two possible explanations. One, rupture of synapses is possible, although unlikely, since we visually ensure the integrity of the neurite

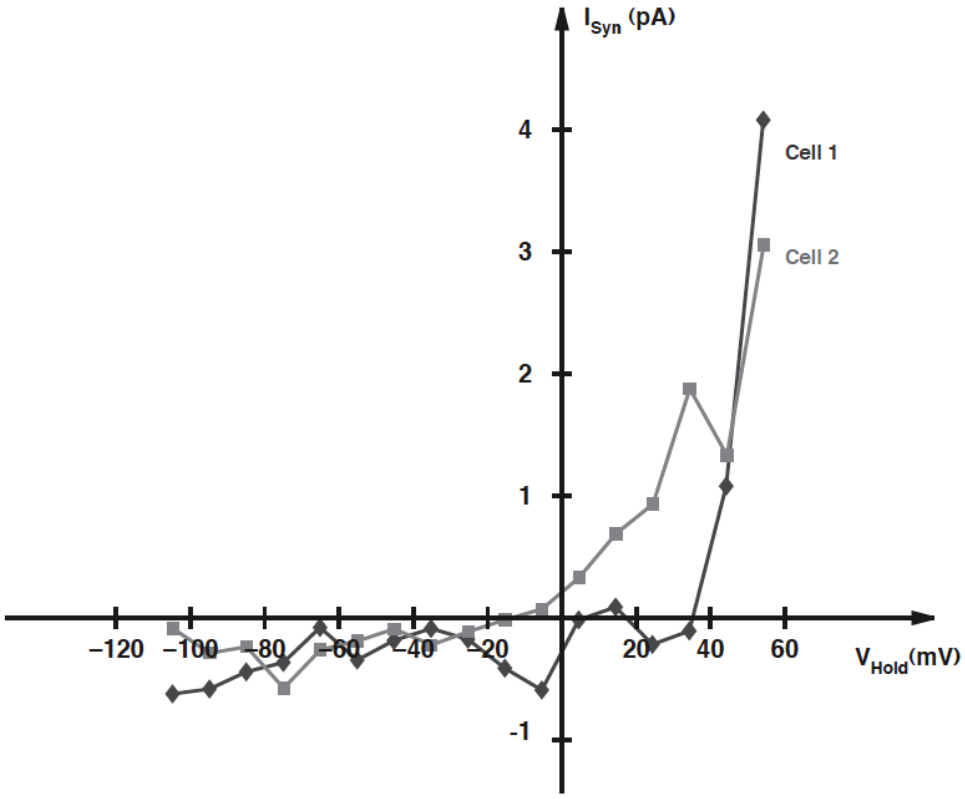

Figure 3.2: Effect of holding potential on the AFD-mediated synaptic current in AIY. Evoked synaptic current, I_{syn} as a function of holding potential, V_{hold}. I-V curves for two neurons. The synaptic current appears to reverse in the range of -20 mV to 0 mV

before commencing recording. Alternatively, it is possible that in some recordings, Cs^+ was not adequately delivered to the synaptic site, although the similar profile of voltage-activated currents in neurons with and without synaptic responses (described further in the following section) indicate that Cs^+ was effective in the soma in both cases. Overall, we cannot conclude substantively whether Cs^+ affected the synaptic response.

3.3 Native voltage activated currents in AIY

The membrane of AIY displayed rich dynamics, showing transients varying in size from a few to tens of millivolts which both depolarized and repolarized the neuron (see Figure 2.4 for examples). We investigated the native voltage-dependent currents exhibited in AIY, by systematically clamping the AIY membrane at different holding potentials and measuring evoked currents (Figure 3.4).

Qualitatively, it would appear that there is at least one inward current and two outward currents activated by depolarization. The inward current is especially prominent at +115 mV, within the first 200 ms of the voltage pulse (also observable by the dip in the I-V curve at +115 mV for 4 out of 5 neurons, Figure 3.4B). The peak evoked current varied four-fold across five cells (Figure 3.4B) as did the steady state current (Figure 3.4C).

We substituted Cs^+ for K^+ in our pipette, to block voltage gated K^+ channels. As mentioned earlier, the synaptic response was abolished in about half the neurons undergoing this substitution. Figure 3.5A shows example traces in voltage clamp

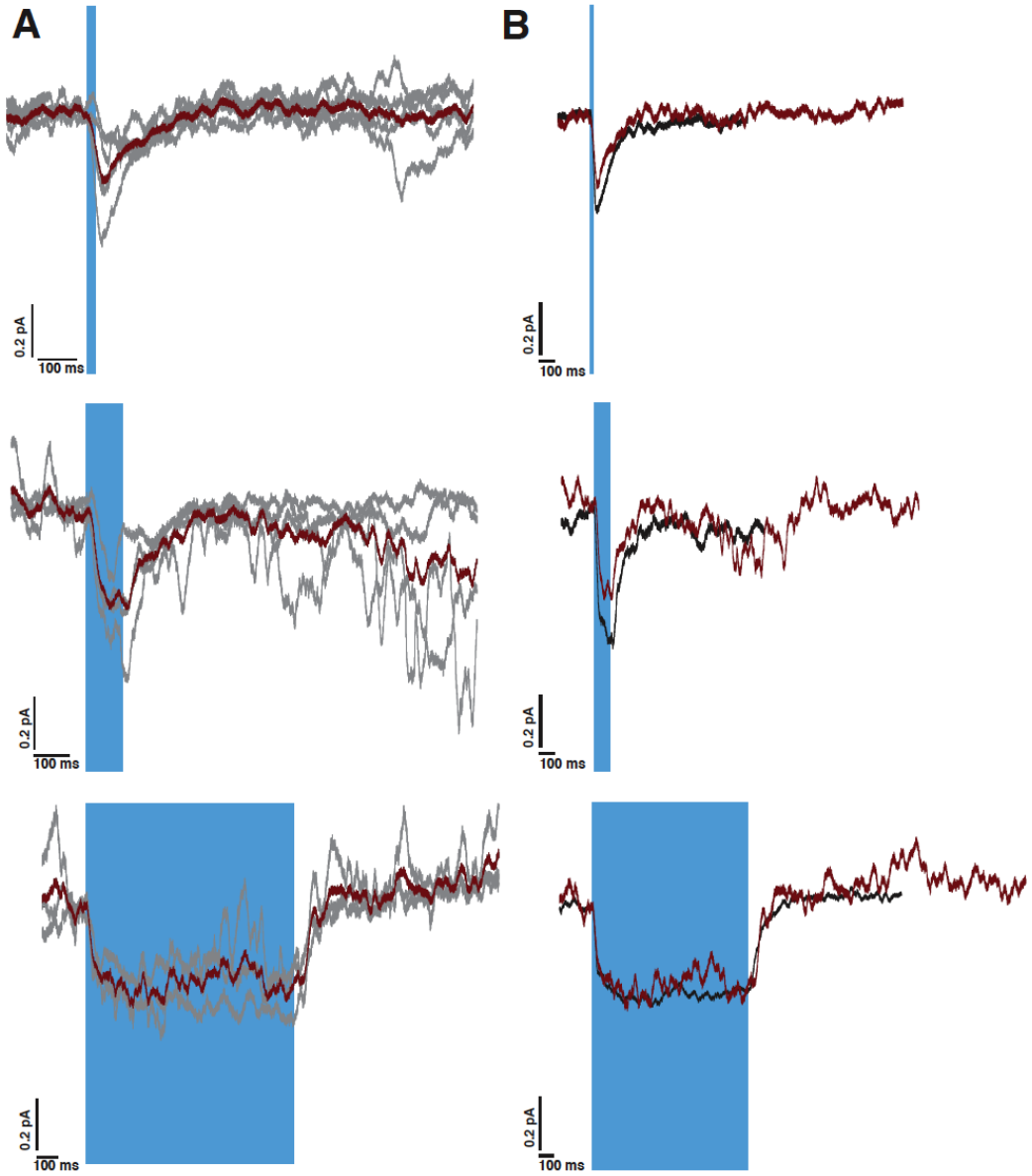

Figure 3.3: No observable effect of Cs^+ on synaptic current. A. Evoked current in AIY in response to 20 ms (top), 100 ms (middle) and 1 s (bottom) blue light stimulation, with Cs^+ substituting for K^+ in the pipette. Gray, 10-trial averages of individual cells, red, average evoked current over all cells. B. No noticeable difference in response with Cs^+ (in red) compared to recordings made with K^+ internal (in black, reproduced from Figure 2.4C).

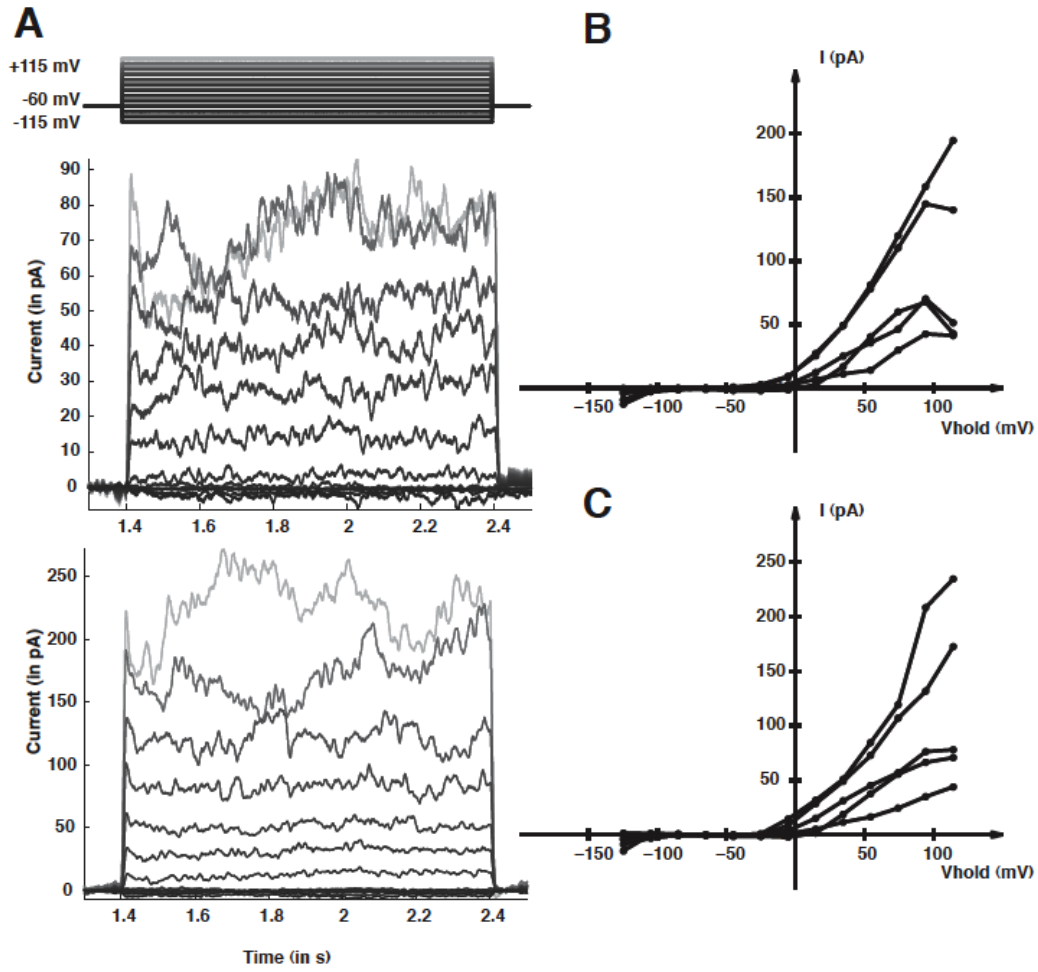

Figure 3.4: Native currents in the AIY membrane A. Response of AIY membrane to 1 second long voltage steps from a holding potential of -60 mV up to +115mV and down to -115 mV. Current responses to each step shown for two cells (top and bottom). B. Individual I-V curves plotted for evoked current within the first 50-150ms of the voltage step and C. the last 100 ms of the voltage step for 5 neurons.

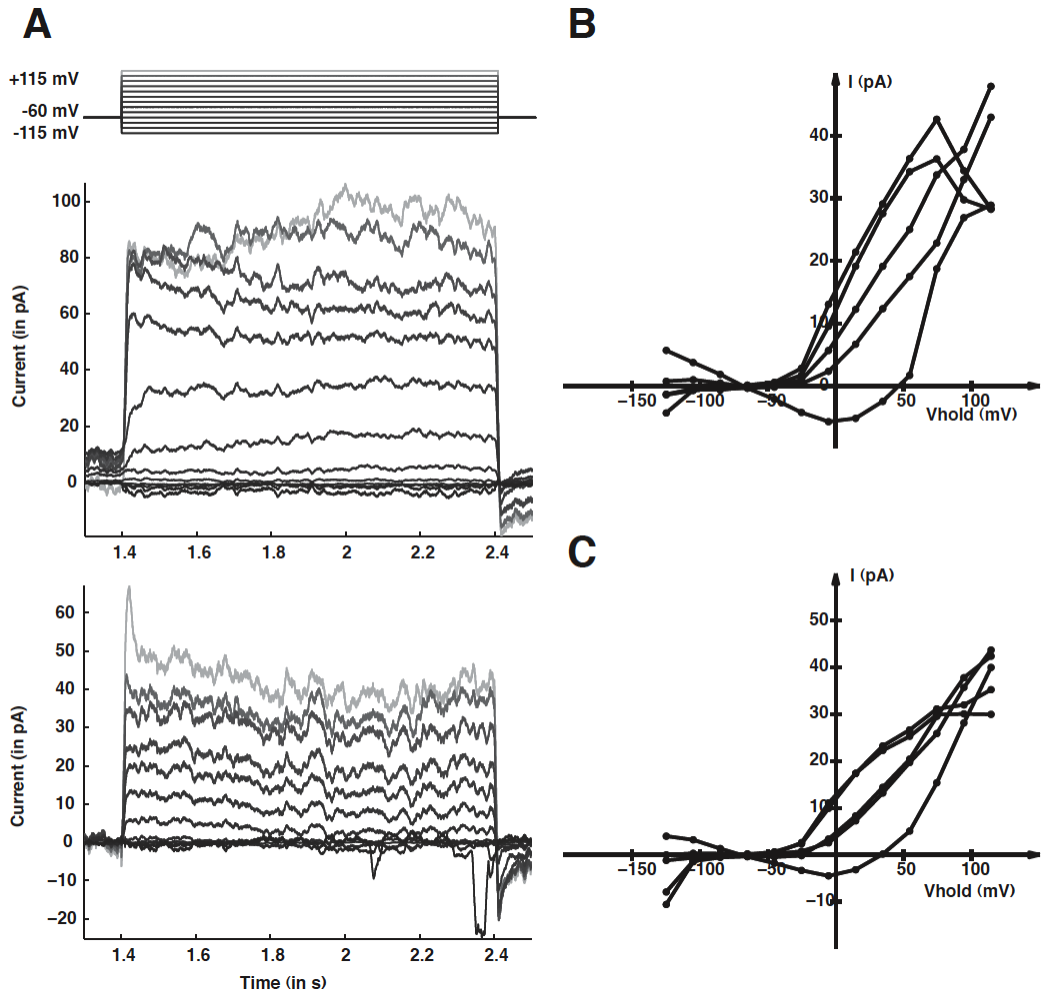

Figure 3.5: Effect of substituting Cs^+ for K^+ on the IV curve A. Response of AIY membrane to 1 second long voltage steps from a holding potential of -60 mV up to +115mV and down to -115 mV. Current responses to each step shown for a neuron exhibiting no synaptic response (top) and a neuron exhibiting synaptic response (bottom). B. Individual I-V curves plotted for evoked current within the first 50-150ms of the voltage step and C. the last 100 ms of the voltage step for 5 neurons exhibiting synaptic responses in the presence of Cs^+ internal.

from a neuron exhibiting no synaptic response (top) and a neuron exhibiting synaptic response (bottom) in response to a series of voltage steps. Figure 3.5B shows evoked current in the first 50-150 ms of the voltage step, versus voltage for 5 neurons exhibiting a synaptic response in the presence of Cs^+ internal. Figure 3.5C shows the evoked current in the last 100 ms of the voltage step for the same 5 neurons. In both cases, the range of the evoked current was reduced by a quarter compared to the K^+ case in Figure 3.4, indicating that a substantial fraction of the outward current is carried by K^+.

In all cases, current responses were P/N subtracted to remove leak and capacitive currents.

3.4 Spontaneous events in AFD, AIY and ASER

We also assessed the effect of current injections of varying magnitude on the membrane of different cells - AFD, ASER, and AIY. Figure 3.6 shows one example of the membrane of ASER to current injections of varying amplitude. As the membrane was more depolarized, voltage activated non-linearities were exhibited by the membrane, and the sharp individual psps seen at more hyperpolarized membrane potential values gradually reduced in number. There are at least two possible explanations. It is possible that these events represent the opening and closing of single ion channels which are activated by hyperpolarizing membrane potentials. In that case, as the membrane is depolarized, the frequency of such events goes down. Another possibility is that these events are synaptic potentials. Hyperpolarizing the membrane

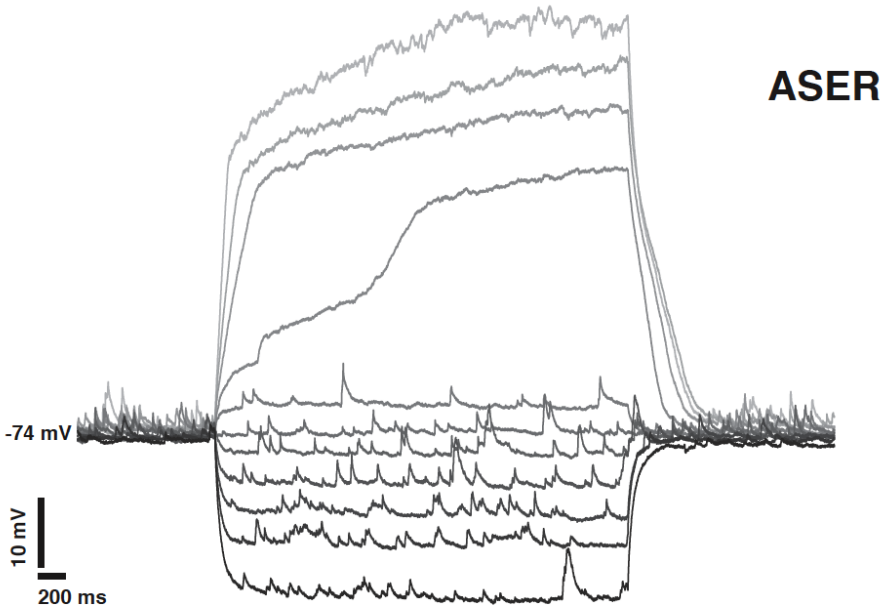

Figure 3.6: Spontaneous events in ASER The ASER membrane exhibits a range of voltage dependent behavior in response to current injections ranging from +5 pA to -5 pA from holding current (the current needed to keep the cell at -74 mV.) The presence of small psp-like events is notable.

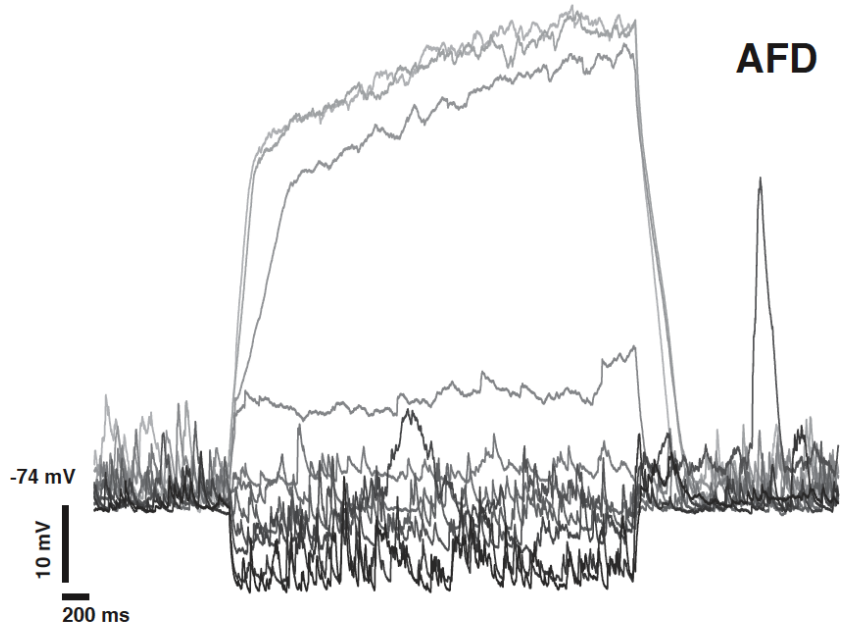

Figure 3.7: Spontaneous events in AFD

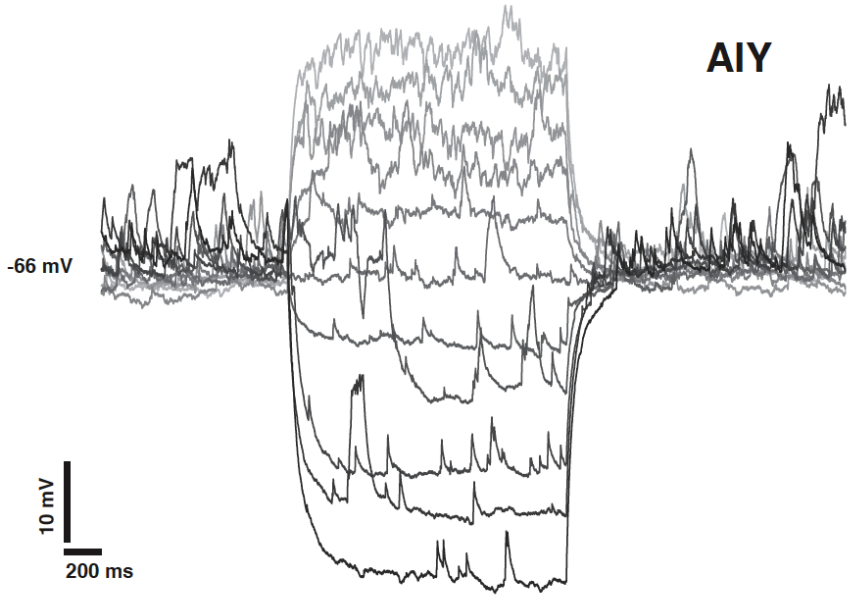

Figure 3.8: Spontaneous events in AIY in response to current injections ranging from +5 pA to -5 pA from holding current

reduces other voltage-activated currents, revealing these events. As the membrane is depolarized, the synaptic potentials should start to reverse. We cannot discern clear reversals. One possible explanation could be the fact that at depolarizing potentials other voltage gated currents are activated, making it challenging to isolate individual synaptic events. To test if these events are synaptic in origin, we recorded from the same neurons in an *unc-13 (s69)* mutant background. *Unc-13* is a syntaxin-binding protein and *unc-13* mutants have significantly reduced synaptic transmission (Richmond et al., 1999). We found significant reduction in frequency of such events (see Figure 2.5) in ASER. We conclude that at least a fraction of these psp-like events are synaptic in origin.

Such events were seen in AFD as well (see Figure 3.7) , and the AFD membrane exhibited sharp active charging curves at more depolarized membrane. The same

held true for AIY (Figure 3.8). In addition, AIY appeared to exhibit a wider range of sizes and kinetics for the evoked psps, suggesting a greater diversity of sources of synaptic input.

3.5 Discussion

The synaptic current evoked in AIY through light-evoked depolarization of AFD was small and appeared to reverse in the range of -20 mV to 0 mV; this is consistent with a current carried by a mixed-cationic conductance. The synaptic current was either abolished or unchanged when Cs^+ was substituted for K^+ in the patch pipette, leaving the effect of Cs^+ upon the synaptic current unresolved. However, voltage dependent outward currents in AIY were reduced fourfold when Cs^+ was substituted for K^+, indicating that a large fraction of the voltage activated outward current appears to be K^+ mediated. The membrane of AFD, AIY and ASER all exhibit a variety of voltage dependent potentials, and a high incidence of psp like events, at least a fraction of which are synaptic in origin. We conclude that the membrane of these neurons in *C. elegans* exhibit rich dynamics that help shape their response to input.

Chapter 4

Transfer at a chemosensory synapse in *C. elegans*

The worm is known to navigate towards certain cues and away from others; this behavior presumably allows it to find food and mates. Sensory information from the external environment is transduced through a set of sensory neurons, processed through layers of interneurons, and finally affect the behavior of the worm by directing movement toward or away from the stimulus. In Chapter 2 we described one form of sensory response exhibited by the worm, thermotaxis; in this chapter we discuss another: the ability to navigate chemical gradients, chemotaxis.

4.1 The circuit for chemotaxis and the ASER-AIY synapse

Chemical sensation is an important mechanism by which *C. elegans* explores and navigates its environment. Worms can chemotax towards peak of gradients of ions and molecules such as Na^+, and K^+, cAmp and lyseine (Ward, 1973). This ability

allows the worm to position itself in a more favorable environment, and represents the culmination of a sequence of neural transformations to motor output, starting with the representation of the chemical environment in the sensory neuron layer.

There are 11 classes of chemosensory neurons in *C. elegans*. Laser ablation studies have shown that their tuning curves overlap redundantly to a variety of small molecules both organic and inorganic (Bargmann & Horvitz, 1991). The class ASE belongs to this group, and ablation of these neurons reduced the animals ability to chemotax towards salts to a much higher degree than ablations of other neurons.

Studies have shown that the anatomically homologous pair ASER and ASEL exhibit striking asymmetries in gene expression (Yu et al., 1997)and ion sensitivities (Pierce-Shimomura et al., 2001). ASEL is primarily sensitive to sodium, while ASER to potassium and chloride ions. Focal laser ablations of ASER disrupts chloride chemotaxis, while ablating ASEL reduces sodium chemotaxis. Additionally, calcium imaging experiments show that ASEL is an ON-cell: increases in sodium chloride concentrations stimulate it; while ASER, stimulated by decreases in sodium chloride concentrations, is an OFF-cell (Suzuki et al., 2008). This difference in sensitivities has an expected effect on behavior: Activation of ASEL promotes runs (bouts of forward locomotion) while activation of ASER promotes turns (implying direction changes).

It appears, therefore, that these neurons compute a time derivative of concentration changes, which is then processed by downstream interneurons, and ultimately signals the motor command interneurons to directs movement towards or away from the stimulus.

ASER has several post-synaptic partners, the most prominent of which are the interneurons AIB and AIY (as described in (Chen et al., 2006), from electron microscope data in (White et al., 1986)). Genetic ablation of AIY reduces the reversal frequency upon exposure to cAMP (sensed through ASE), which suggests that AIY is involved in mediating the response to input transduced through ASE (Tsalik & Hobert, 2003). We began our attempt to track the flow of chemosensory information originating from a single neuron, ASER, by focusing on the synapse between ASER and AIY. In this, we were aided by the fact that cell-specific promoters for both ASER and AIY exist (*gcy-5* and *ttx-3* respectively). Our methods were similar to those described in Chapter 2. We stimulated ASER by the selective expression of channelrhodopsin-2 in that cell, visualized ASER and AIY by the selective expression of gfp, and recorded currents and potentials in ASER and AIY using whole-cell patch clamp.

4.2 Results

4.2.1 Activation of ASER using ChR2

We depolarized ASER remotely and selectively by expressing chR2 under the *gcy-5* promoter, which is exclusively expressed in ASER (Yu et al., 1997). Worms were fed the necessary co-factor all-*trans* retinal (ATR). To ensure that ASER was depolarized by our remote light stimulation, we first patched onto ASER and recorded light-evoked whole-cell currents and voltage changes. With blue light, we were able to

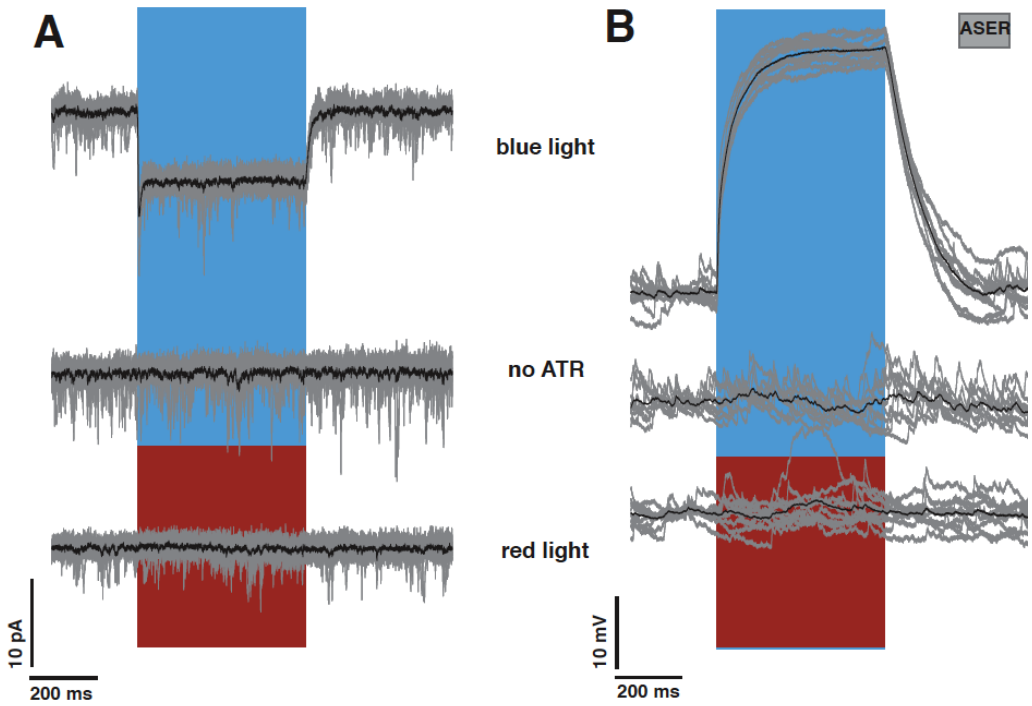

Figure 4.1: Activating ASER using ChR2. Voltage clamp recordings from ASER. A 500 ms pulse of blue light, and not red, causes inward current in ASER expressing functional chR2. All-*trans* retinal is required. 10 trials from a single neuron in gray, average in black. V_{Hold} = -65 mV. D. Current Clamp recordings from AFD in situations identical to (C). V_{Hold} = ∼-70 mV

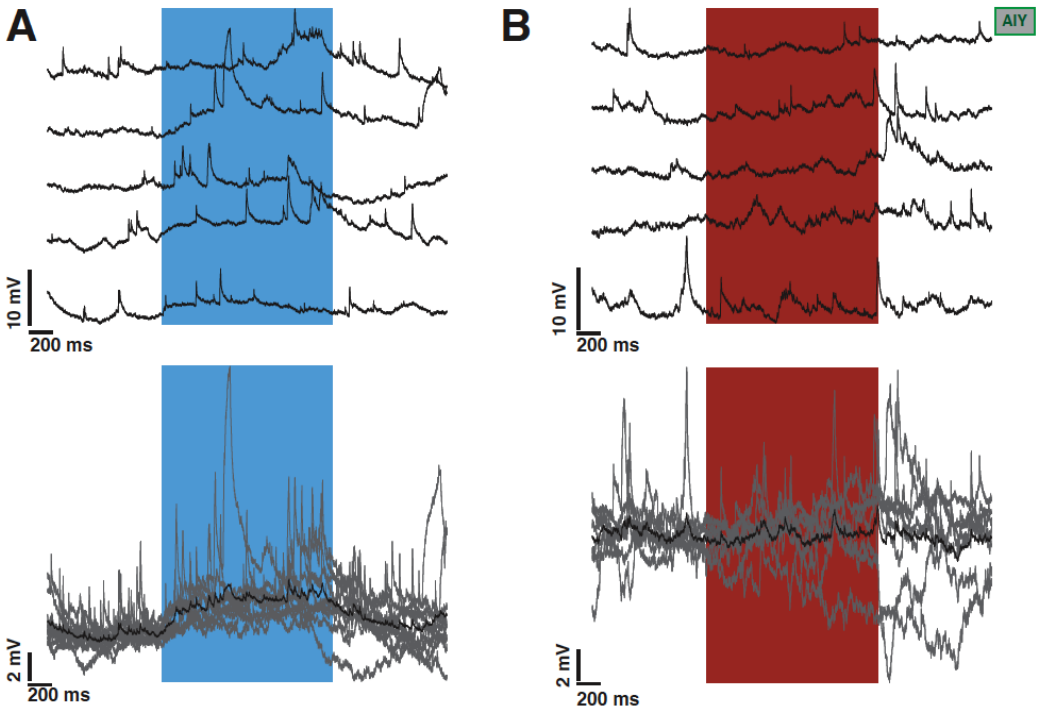

Figure 4.2: AIY voltage response to ASER stimulation A. Current clamp recordings from AIY in response to a 1 second long pulse of blue light. 5 example trials from one neuron, top (black), overlay of 10 trials from same neuron (gray) with average (black), bottom. V_{Hold} = ∼-70 mV. B. Current clamp recordings from AIY in response to red light, 5 individual trials, top, 7 trials (gray) overlaid with average (black), bottom. V_{Hold} = ∼ -65 mV.

evoke currents up to 10 pA and depolarizations up to 40 mV (Figure 4.1A). Control experiments with red light or using worms fed no ATR showed no response (Figure 4.1B). The response was reliable and reversible.

4.2.2 Response in AIY to ASER activation

Having ensured that our light stimulation does indeed depolarize ASER, we next recorded responses from AIY to blue light stimulation. With 1 s pulses of blue light, we occasionally saw a small depolarization in AIY. Figure 4.2A shows example traces from one neuron in which we saw a slight response. Figure 4.2B shows the response

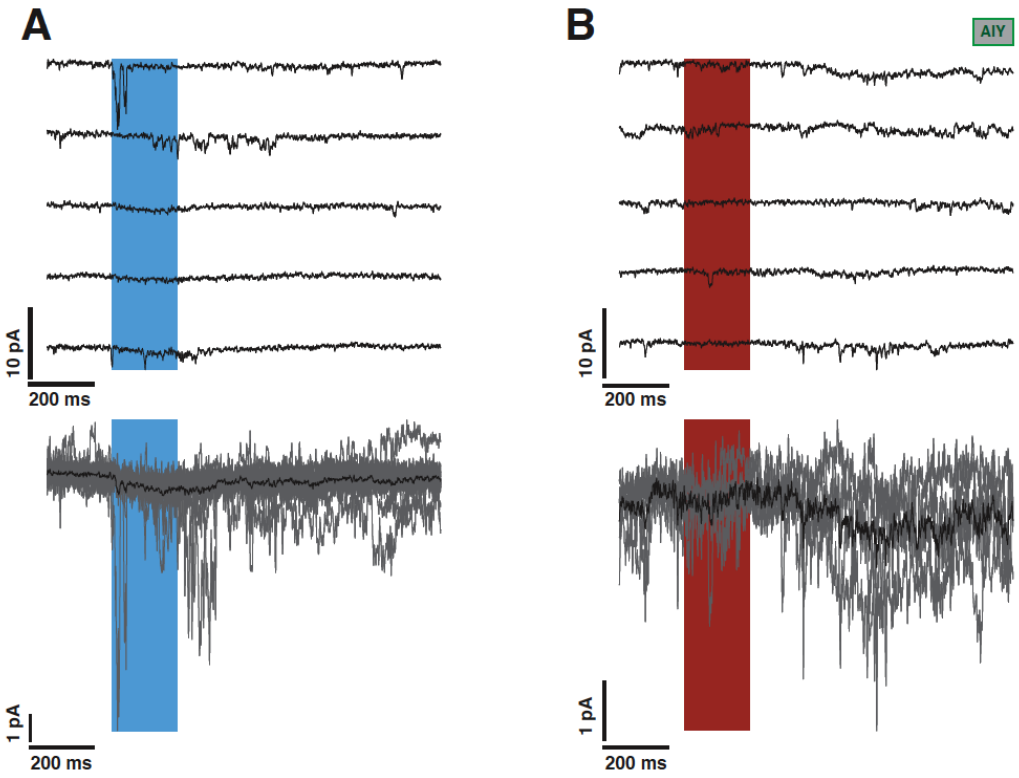

Figure 4.3: AIY current response to ASER stimulation. A. Voltage clamp recordings from AIY in response to a 200 ms long pulse of blue light. 5 example trials from one neuron, top (black), overlay of 20 trials from same neuron, bottom (gray), average of 20 trials, bottom (black). V_{Hold} = -65 mV. B. Voltage clamp recordings from AIY in response to red light, 5 individual trials, top, 5 trials (gray) overlaid with average (black), bottom. V_{Hold} = -65 mV.

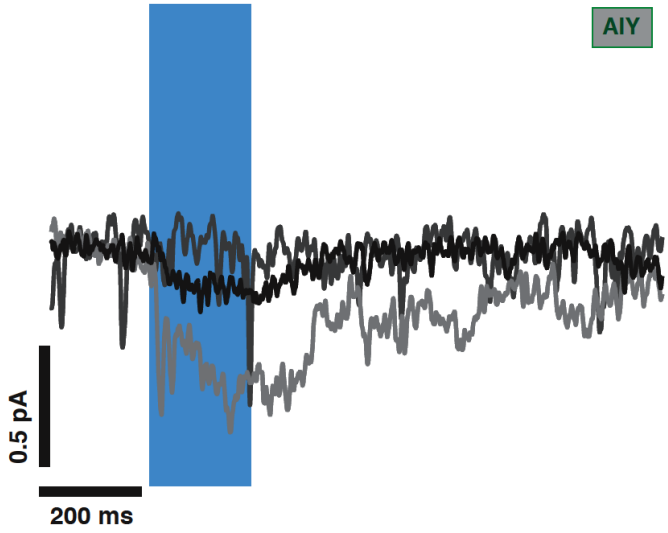

Figure 4.4: AIY response to ASER stimulation is not consistent. Voltage clamp recordings from AIY in response to 200 ms pulse of blue light. 20-trial averages from 3 different cells. V_{Hold} = -65 mV.

of the same neuron to red light pulses, which produce no depolarization. We repeated the experiment in voltage clamp with 200 ms light pulses, to similar effect (Figure 4.3). A small current of < 0.1 pA was occasionally observed. This response was very variable, however, and in most of our recordings, we were not able to identify it clearly. Figure 4.4 shows the average current evoked by a 200 ms blue light pulse in three different cells, with the time courses and amplitudes of evoked current varying widely. Most of our recordings showed no response.

4.3 Discussion

The ASER-AIY synapse is a prominent one: both behaviorally, given its role in the chemotaxis circuit, and structurally, given the large number of points of synaptic contact (determined by electron microscope studies by White et al. (1986)) between ASER and AIY. It is therefore puzzling that the recorded physiological response in

AIY to ASER stimulation should be so small, and in most cases, absent. There could be several reasons for this. First, we must consider whether a 30-40 mV depolarization in ASER from -65 mV (presumed resting potential of the cell) is adequate to trigger neurotransmitter release. This might not be the case: ASER might have a different resting potential (higher or lower than -65 mV) in which case the evoked depolarization could be significantly different; the evoked depolarization, which is limited by the expression and conductance of the chR2 channel, might not be sufficient to trigger release; and the time course and kinetics of the presynaptic chR2-evoked depolarization might not mimic those required for neurotransmitter release at this synapse. Second, it is possible that synapses are ruptured in our preparation. However, we know that at least some synaptic input is retained in our recordings (psp-like events in ASER are significantly diminished in an *unc-13(s69)* synaptic mutant background - see Figure 2.5 and also Figure 3.6). Also similar recordings performed from AIY in response to chR2 stimulation of AFD showed consistent, albeit small, synaptic currents and potentials (see Chapter 2 and 3). Third, ASER is known to be sensitive to the concentration of Cl^- ions, with chemotaxis behavior saturating at $\sim$100 mM concentrations. Since the animal is bathed in extracellular saline with Cl^- concentrations on the order of 150 mM, it is possible that in our recordings ASER is already saturated in its response. Recordings from ciliary mutants that render ASER insensitive to external salt concentrations might be one possible workaround to this problem. Fourth, it is known that worms have an aversive response to long (>1s) pulses of blue light mediated through the *lite-1* Ca^+ channel. Since we use blue light

to both stimulate the synapse and to visualize gfp for our recordings, we might be unintentionally triggering other pathways that affect our measurements. We performed recordings from AIY expressing a red fluorescent protein, ds-red instead of gfp, with short light pulses, we did not see any significant change in our responses. Fifthly, the synaptic current might be shunted away from the AIY cell body and hence not visible at our pipette (as discussed earlier in Chapter 2). Sixth, it is possible that the synaptic response at AIY requires neuromodulators that are not circulating in our semi-intact preparation.

It will be intriguing to explore these issues further, either using ciliary mutants to prevent saturation of ASER, or by hyperpolarizing ASER to see if AIY is affected (using, possibly, halorhodopsin). It will also be interesting to follow the circuit downstream of AIY, to see if synaptic responses not visible at our pipette are in fact capable of eliciting transmitter release from AIY in its turn. Although we were unable to evoke a clear and consistent synaptic response in AIY to ASER stimulation using chR2, we find that the use of remote optical stimulation techniques can effectively replace the need for multiple simultaneous recordings in many cases, making experiments such as ours possible in the first place.

4.4 Contributions

This project was undertaken as a collaboration with Tod Thiele and Shawn Lockery of the University of Oregon, Eugene. The strain XL103 *ntIs8[gcy-5::ChR2, elt-2::gfp]* was constructed by Tod Thiele. Anusha Narayan performed the electrophysiological

experiments.

Chapter 5

Conclusions and future directions

Armed with a static wiring diagram, genetic and laser ablation tools and multiple ways to stimulate and read out neural activity including electrophysiology, and optical imaging, the *C. elegans* nervous system is an attractive one for the study of neuronal communication. To truly understand the neural processing and control of behavior we need a functional wiring diagram. Characterizing transfer at individual synapses is a necessary first step before understanding functional transformation in *C. elegans* neural circuits. We attempted to characterize transfer at two sensory synapses in the worm, and found a combination of optogenetic stimulation techniques with physiological recordings a useful technique, allowing us to control individual neurons with high specificity. Our study was the first of its kind in attempting to characterize transfer at central synapses in *C.elegans*.

5.1 Characteristics of transfer at worm synapses

We found that the thermosensory synapse between AFD-AIY exhibits excitatory, graded and tonic release. It has low gain (< 0.1). This protects AIY from saturation

by a single input channel and and allows it to monitor and integrate multiple input streams, which is consistent with the current picture of the integrative role of AIY, which receives input from a variety of sensory neurons. Release can be maintained for several tens of seconds, making it a highly reliable mechanism for conveying temperature difference information from AFD to AIY. We expect each *C. elegans* synapse to be different; in addition to characterizing a thermosensory synapse we also investigated the chemosensory synapse from ASER to AIY. We found it difficult to reliably evoke a synaptic response in AIY by ASER stimulation. The response, when it did occur, was variable and small, despite the fact that the wiring diagram suggests a high degree of connectivity between ASER and AIY. It is possible that release at the ASER-AIY synapse is more stochastic; it is possible that neuromodulatory or conjunctive sensory input is necessary for AIY to respond to ASER. Much therefore remains to be done to understand the functional activation of neural pathways in *C.elegans*.

5.2 Future directions

Our results from the study of the AFD-AIY synapse suggest some intriguing questions regarding the mechanisms of information integration at AIY. It will be interesting to track the flow of thermosensory information downstream, to other neurons in the circuit such as AIZ and RIA. Additionally, the role of neuromodulation and concomitant synaptic input in causing neurotransmitter release in AIY bears investigation. Behavioral assays using optical stimulation techniques might shed light on some of

these questions, as might taking neurons out of the circuit using halorhodopsin.

Our study is the first that combines optogenetic stimulation with electrophysiology to analyse real-time functioning of neural circuits in *C. elegans*. Some of our results - the absence of a consistent response at the ASER-AIY synapse, and the weakness of the response at the AFD-AIY, run counter to what one might expect by estimating synaptic weights from an inspection of the static connectivity maps. We think therefore that this approach is very promising, and that the analyses of other synapses in the worm using similar techniques will help illuminate the general principles by which this small neural system encodes information and shapes a worm's response to its environment.

Bibliography

Airan, R. D., Thompson, K. R., Fenno, L. E., Bernstein, H., & Deisseroth, K. (2009). Temporally precise in vivo control of intracellular signalling. Nature, 458, 1025–1029.

Altun, Z., Herndon, L., Crocker, C., Lints, R., & Hall, D. (2002-2009). Wormatlas. http://www.wormatlas.org.

Altun, Z. F. & Hall, D. G. (2008). Handbook of c. elegans anatomy. In Wormatlas. http://www.wormatlas.org/hermaphrodite/hermaphroditehomepage.htm.

Arenkiel, B. R., Peca, J., Davison, I. G., Feliciano, C., Deisseroth, K., Augustine, G. J., Ehlers, M. D., & Feng, G. (2007). In vivo light-induced activation of neural circuitry in transgenic mice expressing channelrhodopsin-2. Neuron, 54, 205–218.

Attwell, D., Borges, S., Wu, S. M., & Wilson, M. (1987). Signal clipping by the rod output synapse. Nature, 328, 522–4.

Bargmann, C. I. & Horvitz, H. R. (1991). Chemosensory neurons with overlapping functions direct chemotaxis to multiple chemicals in c. elegans. Neuron, 7, 729–742.

Bi, A., Cui, J., Ma, Y. P., Olshevskaya, E., Pu, M., Dizhoor, A. M., & Pan, Z. H.

(2006). Ectopic expression of a microbial-type rhodopsin restores visual responses in mice with photoreceptor degeneration. Neuron, 50, 23–33.

Biron, D., Wasserman, S., Thomas, J. H., Samuel, A. D., & Sengupta, P. (2008). An olfactory neuron responds stochastically to temperature and modulates caenorhabditis elegans thermotactic behavior. Proc Natl Acad Sci U S A, 105, 11002–7.

Boyden, E. S., Zhang, F., Bamberg, E., Nagel, G., & Deisseroth, K. (2005). Millisecond-timescale, genetically targeted optical control of neural activity. Nat Neurosci, 8, 1263–8.

Brockie, P. J., Madsen, D. M., Zheng, Y., Mellem, J., & Maricq, A. V. (2001). Differential expression of glutamate receptor subunits in the nervous system of caenorhabditis elegans and their regulation by the homeodomain protein unc-42. J Neurosci, 21, 1510–22.

Burrows, M. (1979). Synaptic potentials effect the release of transmitter from locust nonspiking interneurons. Science, 204, 81–3.

Burrows, M. & Siegler, M. V. (1976). Transmission without spikes between locust interneurones and motoneurones. Nature, 262, 222–4.

Burrows, M. & Siegler, M. V. (1978). Graded synaptic transmission between local interneurones and motor neurones in the metathoracic ganglion of the locust. J Physiol, 285, 231–55.

Chalasani, S. H., Chronis, N., Tsunozaki, M., Gray, J. M., Ramot, D., Goodman,

M. B., & Bargmann, C. I. (2007). Dissecting a circuit for olfactory behaviour in caenorhabditis elegans. Nature, 450, 63–70.

Chen, B. L., Hall, D. H., & Chklovskii, D. B. (2006). Wiring optimization can relate neuronal structure and function. Proc Natl Acad Sci U S A, 103, 4723–8.

Chi, C. A., Clark, D. A., Lee, S., Biron, D., Luo, L., Gabel, C. V., Brown, J., Sengupta, P., & Samuel, A. D. (2007). Temperature and food mediate long-term thermotactic behavioral plasticity by association-independent mechanisms in c. elegans. J Exp Biol, 210, 4043–52.

Chung, S. H., Clark, D. A., Gabel, C. V., Mazur, E., & Samuel, A. D. (2006). The role of the afd neuron in c. elegans thermotaxis analyzed using femtosecond laser ablation. BMC Neurosci, 7, 30.

Clark, D. A., Biron, D., Sengupta, P., & Samuel, A. D. (2006). The afd sensory neurons encode multiple functions underlying thermotactic behavior in caenorhabditis elegans. J Neurosci, 26, 7444–51.

Clark, D. A., Gabel, C. V., Gabel, H., & Samuel, A. D. (2007). Temporal activity patterns in thermosensory neurons of freely moving caenorhabditis elegans encode spatial thermal gradients. J Neurosci, 27, 6083–90.

Colosimo, M. E., Brown, A., Mukhopadhyay, S., Gabel, C., Lanjuin, A. E., Samuel, A. D., & Sengupta, P. (2004). Identification of thermosensory and olfactory neuron-specific genes via expression profiling of single neuron types. Curr Biol, 14, 2245–51.

Cruikshank, S. J., Urabe, H., Nurmikko, A. V., & Connors, B. W. (2010). Pathway-specific feedforward circuits between thalamus and neocortex revealed by selective optical stimulation of axons. Neuron, 65, 230–245.

Davis, R. E. & Stretton, A. O. (1989a). Passive membrane properties of motorneurons and their role in long-distance signaling in the nematode ascaris. J. Neurosci., 9, 403–414.

Davis, R. E. & Stretton, A. O. (1989b). Signaling properties of Ascaris motorneurons: graded active responses, graded synaptic transmission, and tonic transmitter release. J. Neurosci., 9, 415–425.

de Bono, M. (2003). Molecular approaches to aggregation behavior and social attachment. J. Neurobiol., 54, 78–92.

de Bono, M. & Maricq, A. V. (2005). Neuronal substrates of complex behaviors in c. elegans. Annu Rev Neurosci, 28, 451–501.

Douglass, A. D., Kraves, S., Deisseroth, K., Schier, A. F., & Engert, F. (2008). Escape behavior elicited by single, channelrhodopsin-2-evoked spikes in zebrafish somatosensory neurons. Curr. Biol., 18, 1133–1137.

Fatt, P. & Katz, B. (1951). An analysis of the end-plate potential recorded with an intracellular electrode. J Physiol, 115, 320–70.

Feldbauer, K., Zimmermann, D., Pintschovius, V., Spitz, J., Bamann, C., & Bamberg,

E. (2009). Channelrhodopsin-2 is a leaky proton pump. Proc. Natl. Acad. Sci. U.S.A., 106, 12317–12322.

Francis, M. M., Mellem, J. E., & Maricq, A. V. (2003). Bridging the gap between genes and behavior: recent advances in the electrophysiological analysis of neural function in caenorhabditis elegans. Trends Neurosci, 26, 90–9.

Giles, A. C., Rose, J. K., & Rankin, C. H. (2006). Investigations of learning and memory in caenorhabditis elegans. Int. Rev. Neurobiol., 69, 37–71.

Goodman, M. B., Hall, D. H., Avery, L., & Lockery, S. R. (1998). Active currents regulate sensitivity and dynamic range in c. elegans neurons. Neuron, 20, 763–72.

Goodman, M. B. & Lockery, S. R. (2000). Pressure polishing: a method for re-shaping patch pipettes during fire polishing. J Neurosci Methods, 100, 13–5.

Graubard, K. (1978). Synaptic transmission without action potentials: input-output properties of a nonspiking presynaptic neuron. J Neurophysiol, 41, 1014–25.

Graubard, K., Raper, J. A., & Hartline, D. K. (1980). Graded synaptic transmission between spiking neurons. Proc Natl Acad Sci U S A, 77, 3733–5.

Griesinger, C. B., Richards, C. D., & Ashmore, J. F. (2005). Fast vesicle replenishment allows indefatigable signalling at the first auditory synapse. Nature, 435, 212–5.

Hamill, O. P., Marty, A., Neher, E., Sakmann, B., & Sigworth, F. J. (1981). Improved patch-clamp techniques for high-resolution current recording from cells and cell-free membrane patches. Pflugers Arch, 391, 85–100.

Han, X. & Boyden, E. S. (2007). Multiple-color optical activation, silencing, and desynchronization of neural activity, with single-spike temporal resolution. PLoS ONE, 2, e299.

Han, X., Qian, X., Bernstein, J. G., Zhou, H. H., Franzesi, G. T., Stern, P., Bronson, R. T., Graybiel, A. M., Desimone, R., & Boyden, E. S. (2009). Millisecond-timescale optical control of neural dynamics in the nonhuman primate brain. Neuron, 62, 191–198.

Hedgecock, E. M. & Russell, R. L. (1975). Normal and mutant thermotaxis in the nematode caenorhabditis elegans. Proc Natl Acad Sci U S A, 72, 4061–5.

Hobert, O. (2003). Behavioral plasticity in c. elegans: paradigms, circuits, genes. J Neurobiol, 54, 203–23.

Huber, D., Petreanu, L., Ghitani, N., Ranade, S., Hromadka, T., Mainen, Z., & Svoboda, K. (2008). Sparse optical microstimulation in barrel cortex drives learned behaviour in freely moving mice. Nature, 451, 61–64.

Juusola, M., French, A. S., Uusitalo, R. O., & Weckstrom, M. (1996). Information processing by graded-potential transmission through tonically active synapses. Trends in Neurosciences, 19, 292–297.

Kimura, K. D., Miyawaki, A., Matsumoto, K., & Mori, I. (2004). The c. elegans thermosensory neuron afd responds to warming. Curr Biol, 14, 1291–5.

Kuhara, A., Okumura, M., Kimata, T., Tanizawa, Y., Takano, R., Kimura, K. D.,

Inada, H., Matsumoto, K., & Mori, I. (2008). Temperature sensing by an olfactory neuron in a circuit controlling behavior of c. elegans. Science, 320, 803–7.

Kusano, K. (1968). Further study of relationship between pre- and postsynaptic potentials in squid giant synapse. Journal of General Physiology, 52, 326–&.

Laughlin, S. B., Howard, J., & Blakeslee, B. (1987). Synaptic limitations to contrast coding in the retina of the blowfly calliphora. Proc R Soc Lond B Biol Sci, 231, 437–67.

Laurent, G. (1993). A dendritic gain control mechanism in axonless neurons of the locust, schistocerca americana. J Physiol, 470, 45–54.

Liewald, J. F., Brauner, M., Stephens, G. J., Bouhours, M., Schultheis, C., Zhen, M., & Gottschalk, A. (2008). Optogenetic analysis of synaptic function. Nat Methods, 5, 895–902.

Liu, Q., Hollopeter, G., & Jorgensen, E. M. (2009). Graded synaptic transmission at the caenorhabditis elegans neuromuscular junction. Proc Natl Acad Sci U S A, 106, 10823–8.

Llinas, R., Steinberg, I. Z., & Walton, K. (1981). Relationship between presynaptic calcium current and postsynaptic potential in squid giant synapse. Biophys J, 33, 323–51.

Luo, L., Clark, D. A., Biron, D., Mahadevan, L., & Samuel, A. D. (2006). Sensorimo-

tor control during isothermal tracking in caenorhabditis elegans. J Exp Biol, 209, 4652–62.

Marin-Burgin, A. & Szczupak, L. (2000). Processing of sensory signals by a non-spiking neuron in the leech. J Comp Physiol A, 186, 989–97.

Martin, A. R. & Ringham, G. L. (1975). Synaptic transfer at a vertebrate central nervous-system synapse. Journal of Physiology-London, 251, 409–426.

Milo, R., Shen-Orr, S., Itzkovitz, S., Kashtan, N., Chklovskii, D., & Alon, U. (2002). Network motifs: simple building blocks of complex networks. Science, 298, 824–827.

Mohri, A., Kodama, E., Kimura, K. D., Koike, M., Mizuno, T., & Mori, I. (2005). Genetic control of temperature preference in the nematode caenorhabditis elegans. Genetics, 169, 1437–50.

Mori, I. & Ohshima, Y. (1995). Neural regulation of thermotaxis in caenorhabditis elegans. Nature, 376, 344–8.

Mori, I., Sasakura, H., & Kuhara, A. (2007). Worm thermotaxis: a model system for analyzing thermosensation and neural plasticity. Curr Opin Neurobiol, 17, 712–9.

Nagel, G., Brauner, M., Liewald, J. F., Adeishvili, N., Bamberg, E., & Gottschalk, A. (2005). Light activation of channelrhodopsin-2 in excitable cells of caenorhabditis elegans triggers rapid behavioral responses. Curr Biol, 15, 2279–84.

Nagel, G., Ollig, D., Fuhrmann, M., Kateriya, S., Musti, A. M., Bamberg, E., &

Hegemann, P. (2002). Channelrhodopsin-1: a light-gated proton channel in green algae. Science, 296, 2395–2398.

Nagel, G., Szellas, T., Huhn, W., Kateriya, S., Adeishvili, N., Berthold, P., Ollig, D., Hegemann, P., & Bamberg, E. (2003). Channelrhodopsin-2, a directly light-gated cation-selective membrane channel. Proc Natl Acad Sci U S A, 100, 13940–5.

Petreanu, L., Huber, D., Sobczyk, A., & Svoboda, K. (2007). Channelrhodopsin-2-assisted circuit mapping of long-range callosal projections. Nat. Neurosci., 10, 663–668.

Pierce-Shimomura, J. T., Faumont, S., Gaston, M. R., Pearson, B. J., & Lockery, S. R. (2001). The homeobox gene lim-6 is required for distinct chemosensory representations in c. elegans. Nature, 410, 694–8.

Raizen, D. M. & Avery, L. (1994). Electrical activity and behavior in the pharynx of Caenorhabditis elegans. Neuron, 12, 483–495.

Ramot, D., Johnson, B. E., Berry, T. L., J., Carnell, L., & Goodman, M. B. (2008). The parallel worm tracker: a platform for measuring average speed and drug-induced paralysis in nematodes. PLoS ONE, 3, e2208.

Reigl, M., Alon, U., & Chklovskii, D. B. (2004). Search for computational modules in the C. elegans brain. BMC Biol., 2, 25.

Richmond, J. E., Davis, W. S., & Jorgensen, E. M. (1999). Unc-13 is required for synaptic vesicle fusion in c. elegans. Nat. Neurosci., 2, 959–964.

Samuel, A. D., Silva, R. A., & Murthy, V. N. (2003). Synaptic activity of the afd neuron in caenorhabditis elegans correlates with thermotactic memory. J Neurosci, 23, 373–6.

Saviane, C. & Silver, R. A. (2006). Fast vesicle reloading and a large pool sustain high bandwidth transmission at a central synapse. Nature, 439, 983–7.

Schroll, C., Riemensperger, T., Bucher, D., Ehmer, J., Voller, T., Erbguth, K., Gerber, B., Hendel, T., Nagel, G., Buchner, E., & Fiala, A. (2006). Light-induced activation of distinct modulatory neurons triggers appetitive or aversive learning in drosophila larvae. Curr. Biol., 16, 1741–1747.

Siegler, M. V. S. (1984). Local interneurones and local interactions in arthropods. Journal of Experimental Biology, 112, 253–381.

Simmons, P. (1982). Transmission mediated with and without spikes at connexions between large second-order neurones of locust ocelli. Journal of Comparative Physiology A: Neuroethology, Sensory, Neural, and Behavioral Physiology, 147, 401–414.

Simmons, P. (1995). The transfer of signals from photoreceptor cells to large second-order neurones in the ocellar visual system of the locust locusta migratoria. J Exp Biol, 198, 537–49.

Simmons, P. J. (1981). Ocellar excitation of the dcmd - an identified locust interneurone. Journal of Experimental Biology, 91, 355–359.

Simmons, P. J. (1993). Adaptation and responses to changes in illumination by 2nd-

order and 3rd-order neurons of locust ocelli. Journal of Comparative Physiology a-Sensory Neural and Behavioral Physiology, 173, 635–648.

Simmons, P. J. (1999). The performance of synapses that convey discrete graded potentials in an insect visual pathway. J Neurosci, 19, 10584–94.

Sterling, P. & Matthews, G. (2005). Structure and function of ribbon synapses. Trends Neurosci, 28, 20–9.

Sukul, N. C. & Croll, N. A. (1978). Influence of Potential Difference and Current on the Electrotaxis of Caenorhaditis elegans. J. Nematol., 10, 314–317.

Suzuki, H., Thiele, T. R., Faumont, S., Ezcurra, M., Lockery, S. R., & Schafer, W. R. (2008). Functional asymmetry in caenorhabditis elegans taste neurons and its computational role in chemotaxis. Nature, 454, 114–7.

Tsalik, E. L. & Hobert, O. (2003). Functional mapping of neurons that control locomotory behavior in Caenorhabditis elegans. J. Neurobiol., 56, 178–197.

Walrond, J. P., Kass, I. S., Stretton, A. O., & Donmoyer, J. E. (1985). Identification of excitatory and inhibitory motoneurons in the nematode Ascaris by electrophysiological techniques. J. Neurosci., 5, 1–8.

Walrond, J. P. & Stretton, A. O. (1985a). Excitatory and inhibitory activity in the dorsal musculature of the nematode ascaris evoked by single dorsal excitatory motonerons. J. Neurosci., 5, 16–22.

Walrond, J. P. & Stretton, A. O. (1985b). Reciprocal inhibition in the motor nervous system of the nematode ascaris: direct control of ventral inhibitory motoneurons by dorsal excitatory motoneurons. J. Neurosci., 5, 9–15.

Ward, S. (1973). Chemotaxis by the nematode caenorhabditis elegans: Identification of attractants and analysis of the response by use of mutants. Proceedings of the National Academy of Sciences of the United States of America, 70, 817–821.

Watson, A. H. & Burrows, M. (1988). Distribution and morphology of synapses on nonspiking local interneurones in the thoracic nervous system of the locust. J Comp Neurol, 272, 605–16.

Wenick, A. S. & Hobert, O. (2004). Genomic cis-regulatory architecture and trans-acting regulators of a single interneuron-specific gene battery in c. elegans. Dev Cell, 6, 757–70.

White, J. G., Southgate, E., Thomson, J. N., & Brenner, S. (1986). The structure of the nervous system of the nematode caenorhabditis elegans. Phil. Trans. R. Soc. Lond. B, 314, 1–340.

Yu, S., Avery, L., Baude, E., & Garbers, D. L. (1997). Guanylyl cyclase expression in specific sensory neurons: a new family of chemosensory receptors. Proc. Natl. Acad. Sci. U.S.A., 94, 3384–3387.

Zhang, Y., Lu, H., & Bargmann, C. I. (2005). Pathogenic bacteria induce aversive olfactory learning in Caenorhabditis elegans. Nature, 438, 179–184.

Zhang, Y. P. & Oertner, T. G. (2007). Optical induction of synaptic plasticity using a light-sensitive channel. Nat. Methods, 4, 139–141.